UNIVERSITY OF SOUTHERN CALIFORNIA
DEPARTMENT OF CIVIL ENGINEERING

INSTRUMENT CORRECTION FOR A COUPLED TRANSDUCER–GALVANOMETER SYSTEM

by

Elena I. Novikova and Mihailo D. Trifunac

Report No. CE 91-02

Los Angeles, California
July, 1991

TABLE OF CONTENTS

ABSTRACT

Instrument correction of records obtained by a coupled transducer–galvanometer system is necessary to eliminate amplitude and phase distortions. A method for correction of the output from a seismograph or accelerometer with galvanometric registration is described. The procedure involves operations in the time domain only, and can be applied to any digitized record. Example tests are presented showing that a ground motion signal can be adequately reconstructed (for both phase and amplitude) in the frequency band which is wider than the nominal range of typical recordings.

I. INTRODUCTION

Seismological and strong motion measurements require use of a variety of devices with electrodynamic registration. The first systematic description of such devices was presented by Galitzin (1912). Depending on the application, the response of coupled "transducer–galvanometer" system may be required to reproduce displacement, velocity or acceleration of a moving point. By changing the constants of both devices one can obtain a system with the transfer function that represents almost ideal displacement, velocity or acceleration meter in a defined frequency band. "Almost ideal" means that the device has the ability to reproduce the amplitude of the motion of interest in the desired frequency band. However, the phase of the direct instrument output is distorted for all frequencies. This is discussed in Chapter II of this report.

The coupled transducer–galvanometer device is very popular in seismology and in earthquake engineering, and a great number of records is being produced by such devices in different countries. For example, in the Soviet Union, structural vibrations are recorded with the help of multichannel systems based on transducers such as VEGIK (Vibrograph, Electrodynamic, Geophysical Institute, Kirnos), SPM-16 (Seismotransducer, Mechanical), VBP (Vibrograph for Big Displacements), and galvanometers of GB type (Medvedev, 1962). Many seismologists are using transducers VEGIK, SGK and SKM with galvanometers of GB type. Variety of techniques are used to control the response of these systems (Khalturin, 1991; Medvedev, 1962). Strong-motion instruments often used in China are RDZ type devices with galvanometers (Lee and Wang, 1983).

There are certain advantages in using coupled systems, as compared with single degree of freedom devices: a) the ability to get a broad range of amplifications, b) the ability to separate recording and measuring locations, and c) the ability to gather and to write on the same medium (film, paper, magnetic tape) the response of several transducers, attached to different places of the object studied (this simplifies time-matching of the different records). Thus, it is useful to process the records obtained by such devices to be as representative of the ground (or structural) motion and in as broad frequency band as possible. This can be accomplished by careful digitization of these records and application of data processing and correction procedures (Trifunac, 1971; 1972; Lee and Trifunac, 1979a,b; 1984; 1990).

Almost any study of earthquake sources, wave propagation or vibration of structures requires information supplied by the broad frequency range of the spectrum of the recorded motions. In consideration of response of long structures to earthquake excitation and in surface-wave propagation, the long-period end of the Fourier spectrum is of considerable importance. Thus, the need for the information contained in the high and in the low frequency ends of the spectrum motivates us to attempt to broaden the frequency band available for the analyses as much as possible.

The majority of the methods used to test mathematical models of earthquake sources, of wave propagation, or of structural vibration require also accurate information about the phase of the motion throughout the frequency range under consideration.

Thus, it is necessary to correct the direct output of coupled transducer–galvanometer systems for the instrument response. Together with the base line correction procedure (Trifunac, 1971), the instrument correction then gives the opportunity to increase the quality of a large number of records obtained from coupled devices and to use them in various analyses. Lee and Wang (1983) developed an instrument correction procedure on the basis of the approximation available for the Chinese RDZ1-12-66 device.

This report presents a method that can be used to correct the direct response of almost any coupled transducer–galvanometer system. The method essentially is the solution of the system of equations of motion for the coupled device in the time domain. Three numerical differentiations and one integration are used to obtain ground acceleration from the direct output of the system. If velocity or displacement are the quantities of interest, additional integration(s) is (are) required.

The advantage of the time domain solution is that it does not assume periodicity of the signal thus avoiding the distortions that arise in the frequency domain filtering. There are methods which reduce those distortions (Press et al., 1986), but those require additional computer memory. A lot of memory is also required if the record to be corrected is very long. This memory may not be available if the whole procedure is to be performed on a relatively inexpensive personal computer. Of course, Fast Fourier Transform of a time series which cannot fit into the computer memory can be taken, but this requires additional exchange of data between RAM memory and the hard disk, thus eliminating the main advantage of the frequency domain filtering: speed.

Numerical differentiation is known to be a difficult procedure to apply in time-series analysis, but it can be shown that if the high frequency digitization errors are filtered out, then it can work very well. However, because of the large number of filtering procedures involved, the question of the filter's accuracy becomes important. The integration emphasizes low frequencies, so high-pass filtering should follow the integration procedure. Low cut-off frequency of the high-pass filters can cause problems as it becomes equivalent (in its difficulty) to the narrow band-pass filtering. The discussion of the properties of the filters used here and the description of the instrument correction procedure are presented in the Chapter III of this report.

II. TRANSFER FUNCTION OF THE COUPLED SYSTEM

II.1 Transducer as a Single Degree of Freedom System

Let us at first consider a transducer working as single degree of freedom (SDOF) system. The motion of such a device can be described by the equation:

$$\ddot{\theta} + 2\omega_1\xi_1\dot{\theta} + \omega_1^2\theta = -\frac{1}{l_0}\,\ddot{x},$$

where θ designates the angle of rotation away from the equilibrium position (the relative motion of the transducer), ω_1 and ξ_1 are natural frequency and ratio of critical damping of the device, l_0 stands for the generalized length of the pendulum of the transducer and $\ddot{x}$ designates the absolute ground acceleration.

The complex transfer function of this system, $C(\omega)$, between the instrument response θ and the input motion x at a particular frequency ω, is

$$C(\omega) = \frac{1}{l_0}\left(\frac{\omega}{\omega_1}\right)^2 \frac{1}{1-\left(\frac{\omega}{\omega_1}\right)^2 + 2i\left(\frac{\omega}{\omega_1}\right)\xi_1}. \tag{1}$$

Then, for harmonic input, the amplification of the system is $|C(\omega)|$, and the phase shift $\gamma(\omega)$ of the output θ with respect to the input displacement x is

$$\gamma(\omega) = \tan^{-1}\left\{\frac{Im\,[C(\omega)]}{Re\,[C(\omega)]}\right\},$$

where Im and Re mean imaginary and real parts of a complex number. For example, if $x = e^{i\omega t}$, then $\theta = C(\omega)\cdot e^{i\omega t} = |C(\omega)|e^{i(\omega t+\gamma(\omega))}$. Introducing dimensionless frequency, $\eta_1 = \omega/\omega_1$, $C(\omega)$ from Eq. (1) can be rewritten as:

$$C(\omega) = \frac{\eta_1^2}{l_0}\cdot\frac{1}{1-\eta_1^2+2i\eta_1\xi_1}.$$

Suppose that the transducer is to measure the displacement of the point were it is attached. That requires

$$\frac{|\theta|}{|x|} = \frac{|C(\omega)\cdot e^{i\omega t}|}{|e^{i\omega t}|} = |C(\omega)| = \text{ const.}$$

This can be realized when $\eta_1 \to \infty$. Indeed, using Taylor series expansion and taking the limit:

$$\lim_{\eta_1\to\infty}|C(\omega)| = \lim_{\eta_1\to\infty}\frac{(1/l_0)\cdot\eta_1^2}{\left\{(1-\eta_1^2)^2+(2\eta_1\xi_1)^2\right\}^{1/2}} = \lim_{\eta_1\to\infty}\frac{1}{l_0}\left\{1+O\left(\frac{1}{\eta_1}\right)^2\right\}.$$

The last equation shows that, as $\eta_1 \to \infty$, the relative angular motion of the transducer is proportional to the displacement of the moving point with amplification $1/l_0$, and this limit is approached within $(1/\eta_1)^2$. For the phase shift there follows:

$$\lim_{\eta_1 \to \infty} \gamma(\omega) = \lim_{\eta_1 \to \infty} \tan^{-1} \left\{ \frac{2\eta_1 \xi_1}{1 - \eta_1^2} \right\} = \lim_{\eta_1 \to \infty} \pi \cdot \left\{ 1 + O\left(\frac{\xi_1}{\eta_1} \right) \right\}.$$

If the device is to measure velocity, then the proportionality of the response of the device and the input velocity is required, i.e. $|C(\omega)|/\omega =$ const should hold. This can be achieved when $\eta_1 \to 1$ and $\xi_1 \gg 1$. To obtain an accelerometer, one should have $|\theta|/|\ddot{x}| =$ const, or $|C(\omega)|/\omega^2 =$ const, and thus $\eta_1 \to 0$ is required. Putting all this together, one can construct Table 1. Note, that $C(\omega)$ describes angular response of the system, and the Dynamic Amplification Factor (DAF) in Table 1 characterizes its linear response. It is important to emphasize that the phase in the case of the velocity meter cannot be a constant, as it is proportional to the frequency even in the limiting case (when $\eta_1 \to 1$). Coefficient of proportionality includes the damping ratio, so one can improve the nature of the response by making $\xi_1 \gg 1$. However, that leads to a decrease of the amplification of the device. The damping ratio is not so crucial (in this sense) in the cases of a displacement or an acceleration meter, and we do not include it in the term describing the limiting behavior for these two cases (in Table 1). However, ξ_1 should be about 0.6 in the latter two cases to secure the proper behavior of the amplitude response when the frequency of motion approaches the natural frequency of the device. By "proper" behavior we mean no dependence on frequency in as broad frequency range as possible.

To visualize the quantities listed in Table 1, one can look at the amplitude and phase response characteristics of the system. Top row of plots in Fig. 1. represents the amplitude response of the device in terms of the quantity to be measured. More specifically, a) shows the amplification for the displacement meter, i.e the ratio between the amplitude of the response of the device, θ, and the amplitude of the ground (or structure) displacement, x, b) gives the amplification for the velocity meter, i.e. the ratio between the amplitude of the response of the device, θ, and the amplitude of the ground (or structure) velocity, $\dot{x}$, and c) presents the output amplification produced by the accelerometer, i.e. $|\theta|/|\ddot{x}|$. Note that all the plotted quantities have been premultiplied by l_0, and are therefore dimensionless.

The bottom row of the same figure describers the phase of the response relative to the phase of the input function. Note that γ gives the phase shift between the input DISPLACEMENT and the output of the device (see Eq. (1)). However, for the case of a velocity meter, one is interested in the phase shift between the VELOCITY of the ground (or structure) motion and the output of the recorder (which is proportional to the velocity of the input motion). This phase shift is equal to $\gamma - \frac{\pi}{2}$ and this quantity is plotted at the bottom of Fig. 1b). A similar consideration for the accelerometer leads to the conclusion that $\gamma + \pi$ describers the phase shift between the output of the accelerometer and the ACCELERATION of the moving point. The corresponding plot is presented in the bottom part of Fig. 1c.

	Transducer is to measure		
	Displacement	Velocity	Acceleration
Angular response of the system	$\lvert C(\omega)\rvert = \frac{1/l_0 \cdot \eta_1^{\,2}}{\sqrt{\left(1-\eta_1^{\,2}\right)^2 + \left(2\eta_1\xi_1\right)^2}}$ $\lvert C(\omega)\rvert = \frac{DAF_d}{l_0}$	$\frac{\lvert C(\omega)\rvert}{\omega} = \frac{1/l_0 \cdot \eta_1/\omega_1}{\sqrt{\left(1-\eta_1^{\,2}\right)^2 + \left(2\eta_1\xi_1\right)^2}}$ $\frac{\lvert C(\omega)\rvert}{\omega} = \frac{DAF_v}{l_0\omega_1}$	$\frac{\lvert C(\omega)\rvert}{\omega^2} = \frac{1/l_0 \cdot \eta_1/\omega_1^{\,2}}{\sqrt{\left(1-\eta_1^{\,2}\right)^2 + \left(2\eta_1\xi_1\right)^2}}$ $\frac{\lvert C(\omega)\rvert}{\omega^2} = \frac{DAF_a}{l_0\omega_1^{\,2}}$
Dynamic amplification factor (**DAF**)	$DAF_d = \frac{\eta_1^{\,2}}{\sqrt{\left(1-\eta_1^{\,2}\right)^2 + \left(2\eta_1\xi_1\right)^2}}$	$DAF_v = \frac{\eta_1}{\sqrt{\left(1-\eta_1^{\,2}\right)^2 + \left(2\eta_1\xi_1\right)^2}}$	$DAF_a = \frac{1}{\sqrt{\left(1-\eta_1^{\,2}\right)^2 + \left(2\eta_1\xi_1\right)^2}}$
Conditions nessesary to aproach the limit	$\eta_1 \to \infty \qquad \xi_1 \approx 0.6$	$\eta_1 \to 1 \qquad \xi_1 >> 1$	$\eta_1 \to 0 \qquad \xi_1 \approx 0.6$
Amplification in the limit and the limiting behavior	$\frac{1}{l_0}\left\{1+\mathrm{O}(\eta_1)^{-2}\right\}$	$\frac{1}{2l_0\omega_1\xi_1}\left\{1+\mathrm{O}(1-\eta_1)\right\}$	$\frac{1}{l_0\omega_1^{\,2}}\left\{1+\mathrm{O}(\eta_1)^2\right\}$
Phase in the limit and its limiting behavior	$\gamma(\omega) = \pi\left\{1+\mathrm{O}(\eta_1)^{-1}\right\}$	$\gamma(\omega) = \pm\frac{\pi}{2}\left\{\mathrm{O}\left(\frac{1-\eta_1}{\xi_1}\right)\right\}$	$\gamma(\omega) = \left\{\mathrm{O}(\eta_1)\right\}$

Table 1 Transfer function of a transducer as a single degree of freedom system.

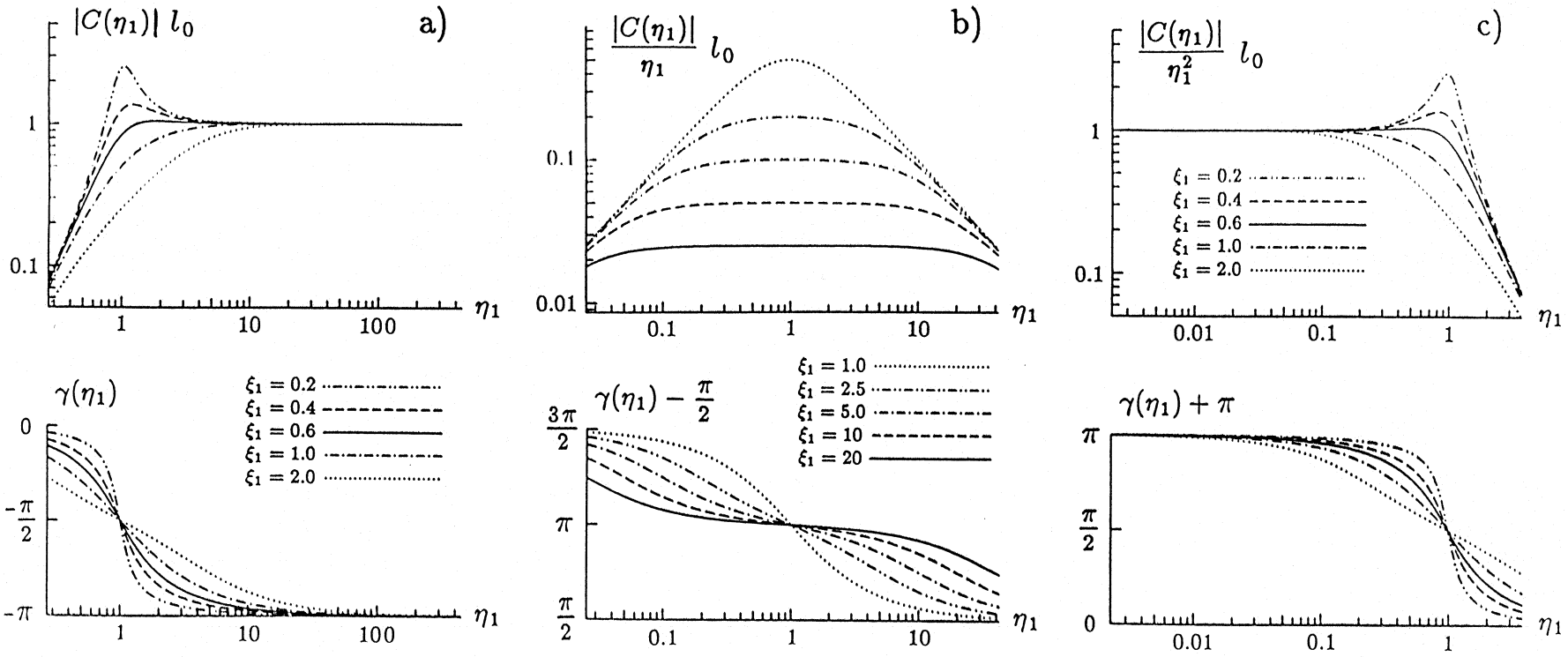

Fig. 1 Transfer function of a SDOF oscillator working as a 1) displacement meter, 2) velocity meter and 3) accelerometer. The plots in the first row show the normalized amplification, and in the second row show the phase shift of the measured quantity.

As it can be seen from Fig. 1, an optimum value of damping ratio, exists for the cases a) and c). When $\xi = 0.6$, the flat portion of the amplitude response (shown in the top row of the figure) extends almost up to the natural frequency of the transducer ($\eta_1 = 1$). In our further considerations we will assume the ratio of critical damping for cases a) and c) to be close to 0.6.

II.2 Response of a Coupled "Transducer–Galvanometer" System

The motion of the coupled system can be represented by the equations:

$$\ddot{\theta} + 2\omega_1\xi_1\dot{\theta} + \omega_1^2\theta = -\frac{1}{l_0}\ddot{x} + 2\omega_1\xi_1\sigma_1\dot{\varphi} \tag{2a}$$

$$\ddot{\varphi} + 2\omega_2\xi_2\dot{\varphi} + \omega_2^2\varphi = 2\omega_2\xi_2\sigma_2\dot{\theta}, \tag{2b}$$

where: θ is the relative rotational response of the transducer,
φ is the response (rotation) of the galvanometer,
ω_1 is the natural frequency of the transducer,
ξ_1 is the ratio of critical damping of the transducer,
ω_2 is the natural frequency of the galvanometer,
ξ_2 is the ratio of critical damping of the galvanometer,
σ_1 is the dimensionless coefficient that describes additional excitation of the transducer due to the feed-back from the galvanometer,
σ_2 is the dimensionless parameter describing the transfer factor for the electrodynamic registration,
l_0 is the generalized length of the pendulum of the transducer,
$\ddot{x}$ is the ground acceleration.

All coefficients involved can be obtained from the physical constants of the transducer and galvanometer (Khalturin, 1991; Borisevich, 1981; Savarensky and Kirnos, 1955).

To get the transfer function of the system, one can assume harmonic excitation with unit amplitude, $x = e^{i\omega t}$, which will result in the harmonic output:

$$\begin{cases} \theta = A(\omega)e^{i\omega t} = |A(\omega)| \cdot e^{i(\omega t + \alpha(\omega))} \\ \varphi = B(\omega)e^{i\omega t} = |B(\omega)| \cdot e^{i(\omega t + \beta(\omega))} \end{cases}. \tag{3}$$

Here $A(\omega)$ designates the intermediate response complex transfer function of the transducer, $B(\omega)$ stands for the complex response of the whole system, $\alpha(\omega)$ represents the phase shift between the input displacement and the intermediate response (of the transducer) and $\beta(\omega)$ is the phase shift between the input displacement and the galvanometer response. Substitution of Eq. (3) into Eq. (2) gives:

$$\begin{bmatrix} 1 - \eta_1^2 + 2i\eta_1\xi_1 & -2i\xi_1\eta_1\sigma_1 \\ -2i\xi_2\eta_2\sigma_2 & 1 - \eta_2^2 + 2i\eta_2\xi_2 \end{bmatrix} \begin{Bmatrix} A(\omega) \\ B(\omega) \end{Bmatrix} = \begin{Bmatrix} \eta_1^2/l_0 \\ 0 \end{Bmatrix}, \tag{4}$$

where the dimensionless frequencies $\eta_1 = \omega/\omega_1$ and $\eta_2 = \omega/\omega_2$ have been introduced. Solution of the system (4) gives both transfer functions:

$$A(\omega) = \frac{\eta_1^2}{l_0} \cdot \frac{a+bi}{c+di},$$
$$B(\omega) = \frac{\sigma_2 \eta_1^2}{l_0} \cdot \frac{bi}{c+di}, \tag{5}$$

where

$$a = 1 - \eta_2^2,$$
$$b = 2\eta_2\xi_2,$$
$$c = (1-\eta_1^2)(1-\eta_2^2) + 4\xi_1\eta_1\xi_2\eta_2(\sigma_1\sigma_2 - 1),$$
$$d = 2\{\eta_2\xi_2(1-\eta_1^2) + \eta_1\xi_1(1-\eta_2^2)\},$$

and amplitude and phase responses:

$$|A(\omega)| = \frac{\eta_1^2}{l_0} \cdot \frac{\{(ac+bd)^2 + (bc-ad)^2\}^{1/2}}{c^2+d^2}, \qquad \tan\alpha(\omega) = \frac{bc-ad}{ac+bd};$$
$$|B(\omega)| = \frac{\sigma_2\eta_1^2}{l_0} \cdot \frac{b}{\{c^2+d^2\}^{1/2}}, \qquad \tan\beta(\omega) = \frac{c}{d}.$$

II.3 Limiting Case for Negligible Coupling

In the case when $\sigma_1 \to 0$, the output from the transducer $A(\omega)$ is very close to the response $C(\omega)$ of the SDOF system, discussed in section II.1. This means that for certain set of parameters the direct transducer output can represent the ground displacement, velocity or acceleration. We examine these three cases in some detail. Later we will summarize the results in the Table 2 and Fig. 2.

II.3.1. Transducer Measures Displacement

Assuming negligible coupling ($\sigma_1 \to 0$), considering the transducer as a displacement meter and using Eq. (2a) together with the Table 1, one can get for the response of the transducer that

$$\text{if } \eta_1 \to \infty, \quad \text{and } \xi_1 \approx 0.6, \qquad \text{then } |A(\omega)| \to \frac{1}{l_0}, \quad \text{and } \alpha(\omega) \to \pi \tag{6}$$

or

$$\theta \propto \frac{1}{l_0} e^{i(\omega t + \pi)} = -\frac{1}{l_0} e^{i\omega t}. \tag{7}$$

The derivative of the response of the transducer represents the excitation for the galvanometer, so, substituting Eq. (7) into Eq. (2b), one obtains the expression for the transfer function of the whole system:

$$B(\omega) = \frac{-1}{l_0} \cdot \frac{2i\xi_2\sigma_2\eta_2}{\{1-\eta_2^2+2i\eta_2\xi_2\}}. \tag{8}$$

The galvanometer is also a SDOF system, so it can also work in three different regimes: it can measure displacement, velocity or acceleration of the input signal. Taking this into consideration, one can ask, if transducer relative response (θ) is proportional to the displacement of the ground, wether it is possible to get the whole "transducer–galvanometer" system to measure a) displacement, b) velocity or c) acceleration of the ground (structural) motion.

a) **Displacement.** Suppose we want $|B(\omega)|$ from Eq. (8) to be proportional to the displacement of the ground, having $|A(\omega)|$ proportional to the ground displacement. That requires

$$|B(\omega)| = \frac{2\xi_2\sigma_2}{l_0} \cdot \frac{\eta_2}{\{(1-\eta_2^2)^2+(2\eta_2\xi_2)^2\}^{1/2}} = \text{const.}$$

Table 1 shows that $\eta_2/\{(1-\eta_2^2)^2+(2\eta_2\xi_2)^2\}^{1/2}$ is $\mathrm{DAF_v}$—dynamic amplification factor for the velocity meter, and this quantity is constant if $\eta_2 \to 1$. This means that, given $|\theta| \propto |x|$, the total response $|\varphi| \propto |x|$ if galvanometer works as a velocity meter, i.e. it has $\eta_2 \approx 1$. Also $\xi_2 \gg 1$ is required to make the amplification and the phase vary less with the frequency of the exitation. This gives for the amplification of the whole system:

$$\lim_{\eta_2 \to 1} |B(\omega)| = \frac{2\xi_2\sigma_2}{l_0} \cdot \frac{1}{2\xi_2} = \frac{\sigma_2}{l_0}. \tag{9}$$

The phase shift, introduced by the galvanometer, is $\pm\frac{\pi}{2}$; shift due to differentiation of θ is $\frac{\pi}{2}$. Recalling the additional phase shift π from the transducer, the total phase shift can be obtained. The phase near $\eta_2 = 1$ is not constant. The phase shift is proportional to the frequency and this is caused by the velocigraph (galvanometer) being involved in the measurement. We will not discuss the phase shift dependence on frequency for all other cases, but it is useful to remember that there is always some reason that causes the phase to "misbehave", that is, to depend on frequency. Amplification in this case is σ_2/l_0, and, as it can be seen from Eq. (2), this factor scales the amplification for all possible sets of devices' constants. To compare amplifications of different systems, one should recall that $l_0 = g/\omega_1^2$, were g is gravitational acceleration on the Earth surface.

b) **Velocity.** Velocity of the ground motion can be obtained if

$$\frac{|B(\omega)|}{\omega} = \frac{2\xi_2\sigma_2}{l_0\omega_2} \cdot \frac{1}{\{(1-\eta_2^2)^2 + (2\eta_2\xi_2)^2\}^{1/2}} = \text{const},$$

which is possible when $\eta_2 \to 0$ (galvanometer is an accelerograph), that is:

$$\lim_{\eta_2 \to 0} \frac{|B(\omega)|}{\omega} = \frac{2\xi_2\sigma_2}{l_0\omega_2}. \tag{10}$$

Notice that $l_0\omega_2$ in the denominator causes the amplification to be small.

c) **Acceleration.** It is not possible to get the whole system to measure acceleration of the ground if the transducer measures displacement. This would require

$$\frac{|B(\omega)|}{\omega^2} = \frac{2\xi_2\sigma_2}{l_0\omega_2} \left\{ \frac{1}{\omega} \frac{1}{[(1-\eta_2^2)^2 + (2\eta_2\xi_2)^2]^{1/2}} \right\} \to \text{const} \cdot (1 + O(\varepsilon))$$

where ε is small. This is impossible because the term $\{\cdot\}$ cannot be represented as const $\cdot (1 + O(\varepsilon))$ in the neighborhood of any of its final limits.

II.3.2 Transducer Measures Velocity

When it is not much distorted by the galvanometer's feed-back ($\sigma_1 \to 0$), the transducer gives the velocity of the ground motion

$$\text{if } \eta_1 \to 1, \quad \text{and } \xi_1 \gg 1, \qquad \text{so that } \frac{|A(\omega)|}{\omega} \to \frac{1}{2l_0\omega_1\xi_1},$$

and

$$\theta(\omega) = i\omega \frac{1}{2l_0\omega_1\xi_1} e^{i\omega t}. \tag{11}$$

Substitution of Eq. (11) into Eq. (2b) gives:

$$B(\omega) = \frac{-\sigma_2}{l_0} \cdot \frac{\xi_2}{\xi_1} \cdot \frac{\omega_2}{\omega_1} \cdot \frac{\eta_2^2}{(1 - \eta_2^2 + 2i\eta_2\xi_2)}.$$

This is the general representation of the transfer function of a system with negligible coupling, if the transducer measures velocity.

a) **Displacement.** The displacement of the ground motion can be obtained if the galvanometer works as a displacement meter, which means that its natural frequency

has to be smaller than the characteristic frequencies of the process being measured. Then

$$\lim_{\eta_2 \to \infty} |B(\omega)| = \frac{\sigma_2 \xi_2 \omega_2}{l_0 \xi_1 \omega_1} \lim_{\eta_2 \to \infty} \frac{\eta_2^2}{\{(1-\eta_2^2)^2 + (2\eta_2 \xi_2)^2\}^{1/2}} = \frac{\sigma_2 \xi_2 \omega_2}{l_0 \xi_1 \omega_1}. \qquad (12)$$

Comparing this amplification with the one from Eq. (9), one can see that $\omega_2 \xi_2 / l_0 \omega_1 \xi_1$ causes the expression in Eq. (12) not to be as small as the expression in Eq. (9), (recall that $l_0 = g/\omega_1^2$, and that ω_1 is small and ω_2 is big when compared to the frequency of motion being measured). However, the pair "transducer (velocigraph) – galvanometer (displacement meter)", resulting in measurement of the displacement of the moving point (designated as $V + D \Rightarrow D$) is seldom used. It is not simple to design a galvanometer with low natural frequency and characteristics stable enough to take advantage of the greater amplification.

b) **Velocity.** The measurement of velocity requires that

$$\frac{|B(\omega)|}{\omega} = \text{const},$$

and this is possible in the arrangement $V + V \Rightarrow V$, which means: transducer measures velocity (of the moving point), galvanometer measures velocity (of the change in the input voltage), and the resultant output is proportional to the velocity of the ground motion. This is possible when $\eta_2 \to 1$, since

$$\lim_{\eta_2 \to 1} \frac{|B(\omega)|}{\omega} = \frac{\sigma_2 \xi_2 \omega_2}{l_0 \xi_1 \omega_1} \cdot \frac{1}{\omega_2} \lim_{\eta_2 \to 1} \frac{\eta_2}{\{(1-\eta_2^2) + (2\eta_2 \xi_2)^2\}^{1/2}} = \frac{\sigma_2}{2 l_0 \xi_1 \omega_1}. \qquad (13)$$

As ω_1 is of the order of the predominant frequencies of the signal being measured, $V+V \Rightarrow V$ (Eq. (13)) is a good combination to "compete" with the pair $D+A \Rightarrow V$ (Eq. (9)) as far as amplification is concerned. However, the limiting behavior of both devices in the pair $V + V \Rightarrow V$ is $O(1-\eta_1)$ and $O(1-\eta_2)$ which makes approaching the limit (constant amplification of the velocity of the moving point) slower, than for the pair $D + A \Rightarrow V$, which has limiting behavior $O\left(1/\eta_1\right)^2$ and $O\left(\eta_2\right)^2$ (in all cases there is a small quantity inside the brackets). This leads to the conclusion that the pair $V + V \Rightarrow V$ can reproduce velocity of the ground motion with relatively small error in narrower frequency band, than the pair $D + A \Rightarrow V$.

c) **Acceleration.** The pair $V + A \Rightarrow A$ gives an output which is proportional to the acceleration of the ground motion. This is achieved when $\eta_2 \to 0$, and the amplification in this case is

$$\lim_{\eta_2 \to 0} \frac{|B(\omega)|}{\omega^2} = \frac{\sigma_2 \xi_2 \omega_2}{l_0 \xi_1 \omega_1} \frac{1}{\omega_2^2} \lim_{\eta_2 \to 0} \frac{1}{\{(1-\eta_2^2)^2 + (2\eta_2 \xi_2)^2\}^{1/2}} = \frac{\xi_2 \sigma_2}{l_0 \xi_1 \omega_1 \omega_2}. \qquad (14)$$

After substitution of the expression for the generalized length l_0, the amplification is seen to be proportional to ω_1/ω_2. This quantity can be small in this particular arrangement; however, having the galvanometer working as an accelerometer makes the amplification very stable.

II.3.3. Transducer Measures Acceleration

The transducer now works as an accelerometer. This means that its natural frequency is bigger than all frequencies involved in the process being measured, that is we will consider

$$\eta_1 \to 0, \quad \text{and } \xi_1 \approx 0.6, \qquad \text{so that} \quad \frac{|A(\omega)|}{\omega^2} \to \frac{1}{l_0\omega_1^2},$$

and

$$\theta(\omega) = \omega^2 \frac{1}{l_0\omega_1^2} e^{i\omega t}. \tag{15}$$

After combining Eqs. (15) and (2b), we obtain following representation of the transfer function of the slightly coupled system in which the transducer measures acceleration:

$$B(\omega) = \frac{2i\xi_2\sigma_2}{l_0\omega_1^2\omega_2} \cdot \frac{\omega^3}{\{(1-\eta_2^2) + 2i\eta_2\xi_2\}}.$$

a) **Displacement.** The displacement output cannot be obtained for the same reason as for the case in paragraph II.3.1 c.

b) **Velocity.** The velocity can be obtained if the galvanometer response is proportional to the displacement, which is the case when $\eta_2 \to \infty$, and then

$$\lim_{\eta_2\to\infty} \frac{|B(\omega)|}{\omega} = \frac{2\sigma_2\xi_2\omega_2}{l_0\omega_1^2} \lim_{\eta_2\to\infty} \frac{\eta_2^2}{\{(1-\eta_2^2)^2 + (2\eta_2\xi_2)^2\}^{1/2}} = \frac{2\sigma_2\xi_2\omega_2}{l_0\omega_1^2}. \tag{16}$$

This pair $(A + D \Rightarrow V)$ appears to be inefficient. Although its amplification is not as small as in the case $D + A \Rightarrow V$ (Eq. (10)), it is difficult to design a galvanometer with stable characteristics and having the natural frequency sufficiently lower than the characteristic frequencies of the ground motion.

c) **Acceleration.** This last case corresponds to the pair $A + V \Rightarrow A$ and represents the most common arrangement of a strong-motion device with galvanometric registration. The amplification of the system with negligible coupling then is:

$$\lim_{\eta_2 \to \infty} \frac{|B(\omega)|}{\omega^2} = \frac{2\sigma_2 \xi_2 \omega_2}{l_0 \omega_1^2} \lim_{\eta_2 \to 1} \frac{\eta_2}{\{(1-\eta_2^2)^2 + (2\eta_2 \xi_2)^2\}^{1/2}} = \frac{\sigma_2}{l_0 \omega_1^2}. \qquad (17)$$

Recalling the definition of the generalized length of the transducer pendulum $l_0 = g/\omega_1^2$, it is seen that the amplification of this device is not small.

II.4 Distortion of the Transducer Response by the Galvanometer Feed-Back

All preceding amplification factors, derived in Section II.3, Eqs. (9), (10), (12)–(14), (16) and (17) were obtained with the assumption that $\sigma_1 = 0$. In this section, we will estimate the "distortion" of the transducer response which is caused by the coupling with a galvanometer, assuming that the transducer is "ideal". Here "ideal" means that the response of the transducer, working alone as a SDOF system, is proportional to either displacement, velocity, or acceleration of the ground. This distortion then can be used to estimate the effect of the coupling on the total response of the system. This is possible because the second device (galvanometer) behaving as a single degree of freedom system (see Eq. (2b)), is a linear system.

The amplification factors discussed in Section II.3 are for no coupling, and therefore can be considered as a zero approximation of the above distortion. Let us now consider the first approximation of the transducer response. We will explain why we call it "first approximation" shortly.

Pair $D+V \Rightarrow D$. In this case the transducer output is proportional to the displacement of the ground, galvanometer works as velocigraph and the whole system measures the displacement of the moving ground or structure. Assuming both devises to be "ideal", for the response of the whole system we have (according to Eq. (9))

$$\varphi = \frac{\sigma_2}{l_0} e^{i\omega t} \qquad \text{with some phase shift.} \qquad (18)$$

Let us consider the magnitude of this function only. Taking advantage of the linearity of the system and substituting Eq. (18) into the equation

$$\ddot{\theta} + 2\omega_1 \xi_1 \dot{\theta} + \omega_1^2 \theta = 2\omega_1 \xi_1 \sigma_1 \dot{\varphi}, \qquad (19)$$

which describes the motion of the transducer due to coupling term alone, we can define the first approximation of the distortion of the transducer due to coupling, as a response of the SDOF system to the exitation $2\omega_1 \xi_1 \sigma_1 \dot{\varphi}$. The total response of the transducer (in time domain) is the sum of its response as a SDOF system and of this first approximation

of the distortion. Having this total response of the transducer, one can get the response of the galvanometer φ, and then repeat the procedure: substitute φ in the Eq. (19) and obtain the second approximation of the distortion of the transducer due to coupling. In this Section, we will restrict ourselves to the consideration of the first approximation of the distortion only, which means we consider "slight" coupling only, $\sigma_1 \approx 0$.

For the case of harmonic exitation, we designate by $A_\sigma(\omega)$ the ratio between the input (ground) displacement $x = e^{i\omega t}$ and the distortion part of the transducer output, i.e. the time domain response to the exitation at the left hand side of Eq. (19), $2\omega_1\xi_1\sigma_1\dot{\varphi}$. We will call $A_\sigma(\omega)$ "the distortion (in the frequency domain)", and will consider only the absolute value of it.

Recall now that we consider the pair $D + V \Rightarrow D$, so we assume $\eta_1 \to \infty$. Then

$$\lim_{\eta_1\to\infty} |A_\sigma(\omega)| = \frac{2\xi_1\sigma_1\sigma_2}{l_0\eta_1} \lim_{\eta_1\to\infty} \frac{\eta_1^2}{\{(1-\eta_1^2)^2 + (2\eta_1\xi_1)^2\}^{1/2}} = \frac{2\xi_1\sigma_1\sigma_2}{l_0\eta_1}.$$

Hence, in the limit, when $\eta_1 \to \infty$, for two "ideal" devices, the distortion of the response of the transducer, slightly coupled with the galvanometer, is proportional to $1/\eta_1$. This distortion is not significant even for considerable coupling $\sigma_1\sigma_2 \approx 1$, since $\eta_1 \to \infty$. However, the distortion of the transfer function of the transducer because of coupling is greater, than the distortion of this function due to "non ideal" characteristics of the transducer (η_1 cannot be infinitely large). While the departure from "ideal" transducer is proportional (see Table 1) to $(1/\eta_1)^2$ (in the case of a displacement meter), the distortion due to coupling is proportional only to $(1/\eta_1)$, and the latter is greater, as $\eta_1 \to \infty$.

Pair $D + A \Rightarrow V$. "Ideal" response gives

$$|\varphi| = \omega \cdot \frac{2\xi_2\sigma_2}{l_0\omega_2},$$

and the distortion term in frequency domain in this regime is

$$\lim_{\eta_1\to\infty} \frac{|A_\sigma(\omega)|}{|\omega|} = \frac{4\xi_1\xi_2\sigma_1\sigma_2\omega_1}{l_0\omega_2}.$$

It is useful to note that the distortion does not depend on frequency in this case. Hence, the coupling just shifts the flat portion of the graph of the response spectrum without disturbing its shape.

Analogous formulae describing distortion of the transducer response for all other possible cases can be obtained in a similar fashion. It appears that the nature of coupling in all arrangements is similar to the one of the two cases described above. In general, the change in the transducer's response due to the feed-back from the galvanometer is similar to the change in the response caused by the change of the critical damping ratio in SDOF system.

Due to linearity of the whole system the distortion of the transducer response will be linearly transmitted through the galvanometer, to the final response of the whole system.

II.5 Summary

It is convenient to summarize all of the above results in a form of Table 2. This table describes all combinations that can be obtained by the pairs of two "ideal" devices, coupled together to measure displacement, velocity or acceleration of the ground motion. Each entry in the table describes one of the possible pairs and gives the needed information:

a) what quantity the output of the system is proportional to (in terms of a short "formula", like $D + V \Rightarrow D$, displacement meter (transducer) and velocigraph (galvanometer) result in the total output being proportional to the displacement),

b) what the amplification factor (Ampl.) is equal to,

c) how significant the distortion of the transducer response due to coupling is (in terms of $|D(\omega) = A_\sigma(\omega)|\ /|A(\omega)|$).

The table also considers the limiting behavior of the transfer function of the SDOF system to estimate the limiting behavior of the coupled system.

Figs. 2a, 2b and 2c complement Table 2 and represent the exact transfer function $B(\omega)$ from Eq. (5) for different arrangements and for different degrees of coupling. Factor $1/l_0$ is omitted in $B(\omega)$ in the Figs. 2a–2c for the purpose of simplicity, thus making all the plotted quantities dimensionless. The case of strong coupling is also presented in Fig. 2 so that the accuracy of the weak coupling approximation can be estimated. Similar to the case of a SDOF system, the amplitude and phase responses with respect to the quantity to be measured are plotted. For the amplitude response, this is the absolute value of the ratio of the measured function of motion (displacement, velocity or acceleration) to the displacement of the moving point. For the phase response, this is the phase lag between x and φ if the displacement is being measured, the phase lag between $\dot{x}$ and $\dot{\varphi}$ if the velocity is being measured and the phase lag between $\ddot{x}$ and $\ddot{\varphi}$ if the acceleration was the quantity of interest. For example, for the output proportional to the acceleration, the top figure in the corresponding pair ($V + A \Rightarrow A$ and $A + V \Rightarrow A$) gives the amplification of the device in terms of the ratio of the measured acceleration to the exact ground acceleration. The phase shift $\gamma + \pi$ gives the delay of the recorded acceleration with respect to the real (input) acceleration.

Table 2 and Fig. 2 show also that small coupling is not necessarily the best choice if the goal is to get the "flat" amplitude response and a constant phase shift in as broad frequency range as possible. As far as the phase is concerned, it is obvious that the ideal case is when $\sigma_1\sigma_2 = 1$, which means complete coupling. In general, small coupling

	Transducer measures displacement: $\eta_1 \to \infty, \quad \xi_1 \approx 0.6$ $O(\eta_1)^{-2}$	Transducer measures velocity: $\eta_1 \to 1, \quad \xi_1 >> 1$ $O(1-\eta_1)$	Transducer measures acceleration: $\eta_1 \to 0, \quad \xi_1 \approx 0.6$ $O(\eta_1)^{2}$
Galvanometer measures displacement: $\eta_2 \to \infty, \quad \xi_2 \approx 0.6$ $O(\eta_2)^{-2}$	Output is proportional to the integral of the displacement of the moving point	$V+D \Rightarrow D$ $\text{Ampl.} = \frac{\sigma_2}{l_0}\frac{\xi_2\omega_2}{\xi_1\omega_1}$ $D(\omega) = \frac{2\sigma_1\sigma_2\xi_2\omega_2}{\omega_1}\frac{1}{\eta_1}$	$A+D \Rightarrow V$ $\text{Ampl.} = \frac{\sigma_2}{l_0}\frac{2\xi_2\omega_2}{\omega_1^2}$ $D(\omega) = \frac{4\sigma_1\sigma_2\xi_1\xi_2\omega_2}{\omega_1}$
Galvanometer measures velocity: $\eta_2 \to 1, \quad \xi_2 >> 1$ $O(1-\eta_2)$	$D+V \Rightarrow D$ $\text{Ampl.} = \frac{\sigma_2}{l_0}$ $D(\omega) = 2\sigma_1\sigma_2\xi_1\frac{1}{\eta_1}$	$V+V \Rightarrow V$ $\text{Ampl.} = \frac{\sigma_2}{l_0}\frac{1}{2\xi_1\omega_1}$ $D(\omega) = \sigma_1\sigma_2$	$A+V \Rightarrow A$ $\text{Ampl.} = \frac{\sigma_2}{l_0}\frac{1}{\omega_1^2}$ $D(\omega) = 2\sigma_1\sigma_2\xi_1\eta_1$
Galvanometer measures acceleration: $\eta_2 \to 0, \quad \xi_2 \approx 0.6$ $O(\eta_2)^{2}$	$D+A \Rightarrow V$ $\text{Ampl.} = \frac{\sigma_2}{l_0}\frac{2\xi_2}{\omega_2}$ $D(\omega) = \frac{4\sigma_1\sigma_2\xi_1\xi_2\omega_1}{\omega_2}$	$V+A \Rightarrow A$ $\text{Ampl.} = \frac{\sigma_2}{l_0}\frac{\xi_2}{\xi_1\omega_1\omega_2}$ $D(\omega) = \frac{2\sigma_1\sigma_2\xi_2\omega_1}{\omega_2}\eta_1$	Output is proportional to the third derivative of the displacement of the moving point

Table 2 Output of the coupled transducer–galvanometer system for various parameters of the transducer and galvanometer when each of them can be approximated by a SDOF system. The letters *D*, *V* and *A* in the "formulae" of the type $D + A \Rightarrow V$ mean displacement, velocity and acceleration respectively. The first term in the left hand side of those "formulae" stands for the type of the transducer (thus, *D* means displacement meter), the second term represents the type of the galvanometer (*A* means accelerometer) and the right hand side of those "formulae" shows what the output of the whole system is proportional to (*V* stands for the output, proportional to velocity of the moving point). The table also presents the amplification of the system in the corresponding limiting case (Ampl.) and the distortion of the transducer due to feed-back from the galvanometer, $D(\omega)$ (see text).

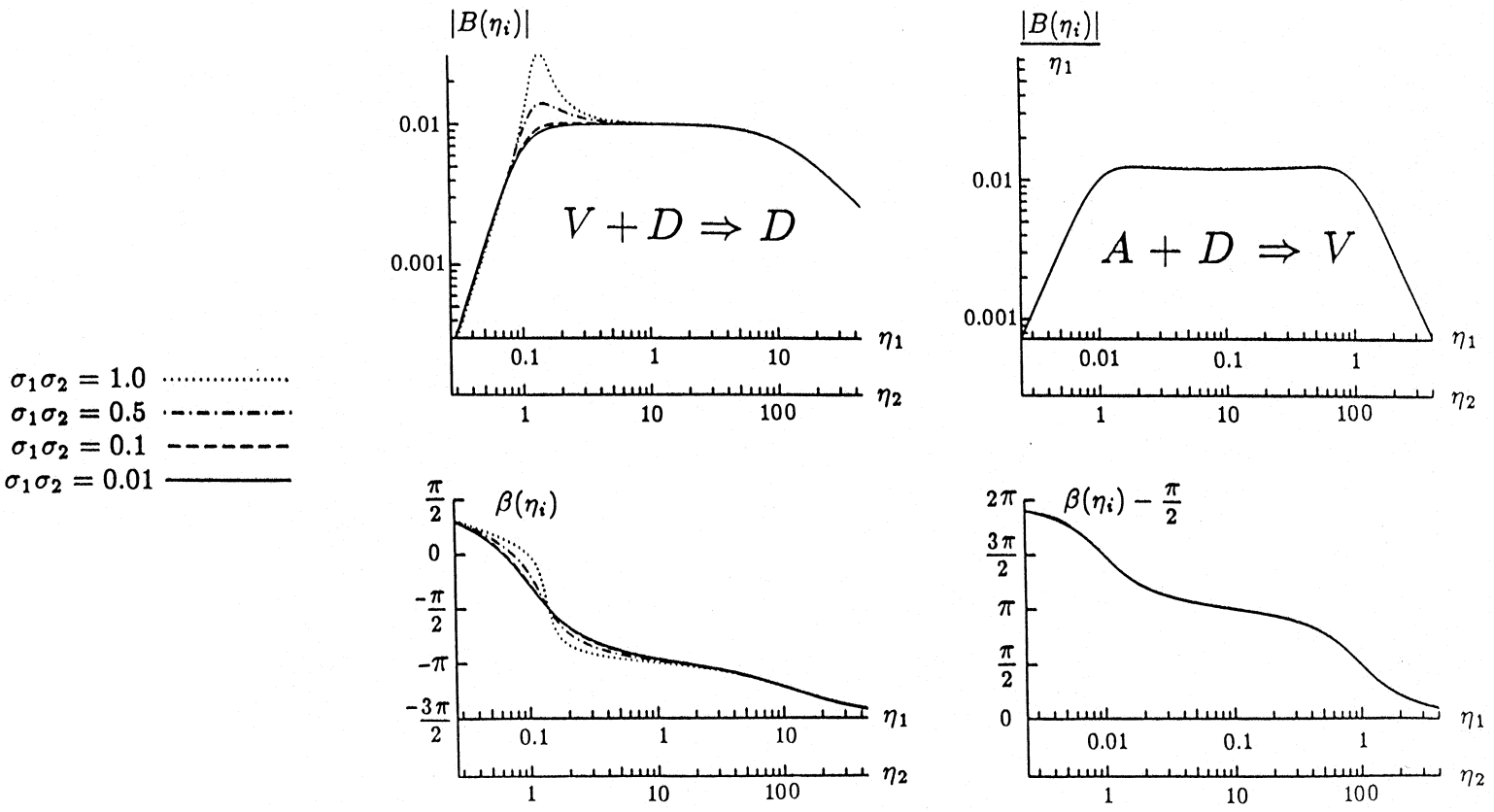

Fig. 2a Transfer function of a coupled transducer–galvanometer system. Case when "galvanometer measures displacement" and left: "transducer measures velocity" ($V+D \Rightarrow D$), right: "transducer measures acceleration" ($A+D \Rightarrow V$); see also the first row in Table 2. The transfer function $B(\eta_1, \eta_2)$ of the coupled system is plotted versus dimensionless frequencies η_1, η_2 for several values of σ_1, ($\sigma_2 = 1$). The critical damping ratios are assumed to be 6.0 for velocity-type device and 0.6 for displacement and acceleration-type devices. The plots in the top of the figure show the normalized amplification, and in the second row show the phase shift of the measured quantity.

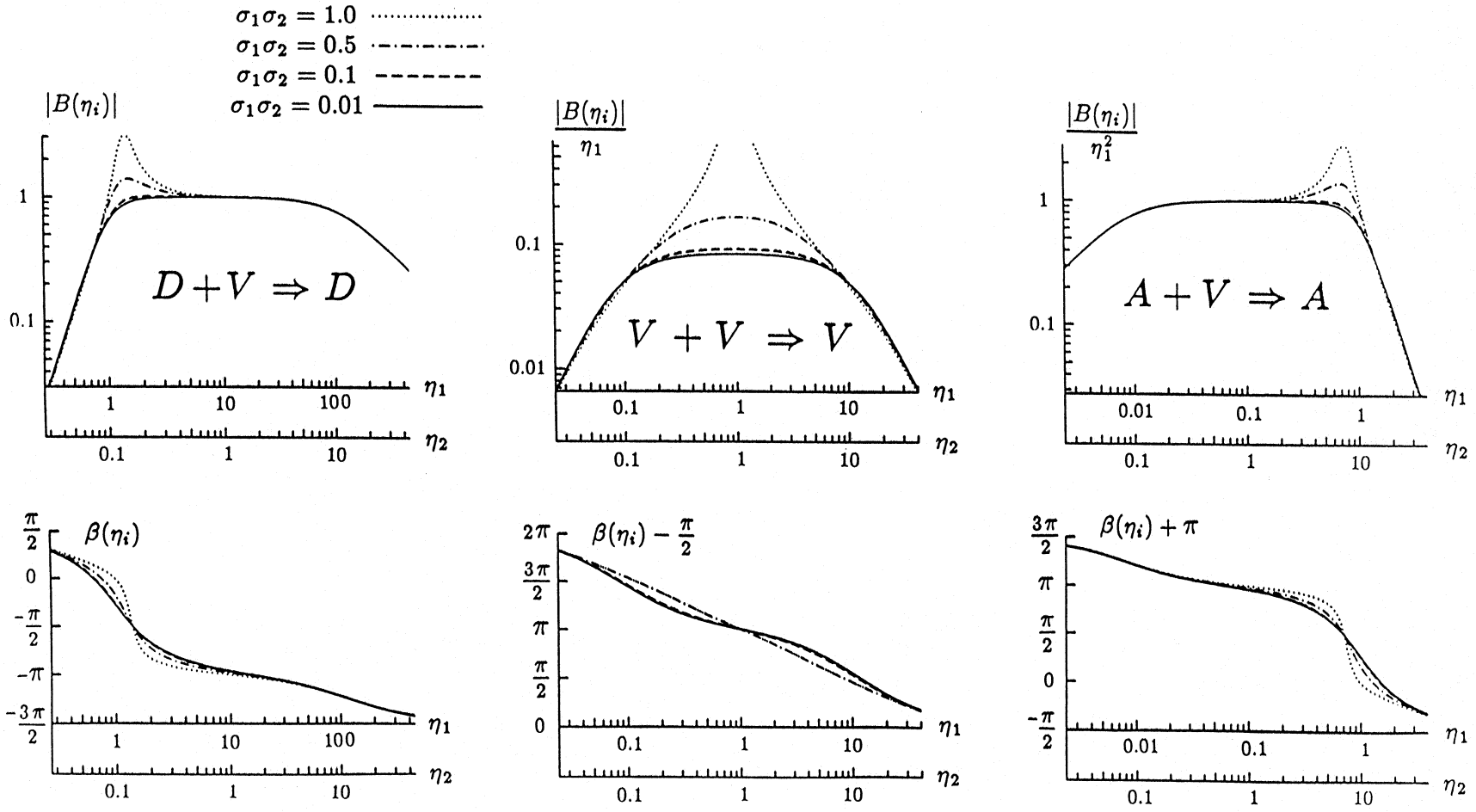

Fig. 2b Transfer function of a coupled transducer–galvanometer system. Case when "galvanometer measures velocity" and left: "transducer measures displacement" $(D+V \Rightarrow D)$, center: "transducer measures velocity" $(V+V \Rightarrow V)$, right: "transducer measures acceleration" $(A+V \Rightarrow A)$; (see also the second row in Table 2). The transfer function $B(\eta_1, \eta_2)$ of the coupled system is plotted versus dimensionless frequencies η_1, η_2 for several values of σ_1, $(\sigma_2 = 1)$. The critical damping ratios are assumed to be 6.0 for velocity-type device and 0.6 for displacement and acceleration-type devices. The plots in the top of the figure show the normalized amplification, and in the second row show the phase shift of the measured quantity.

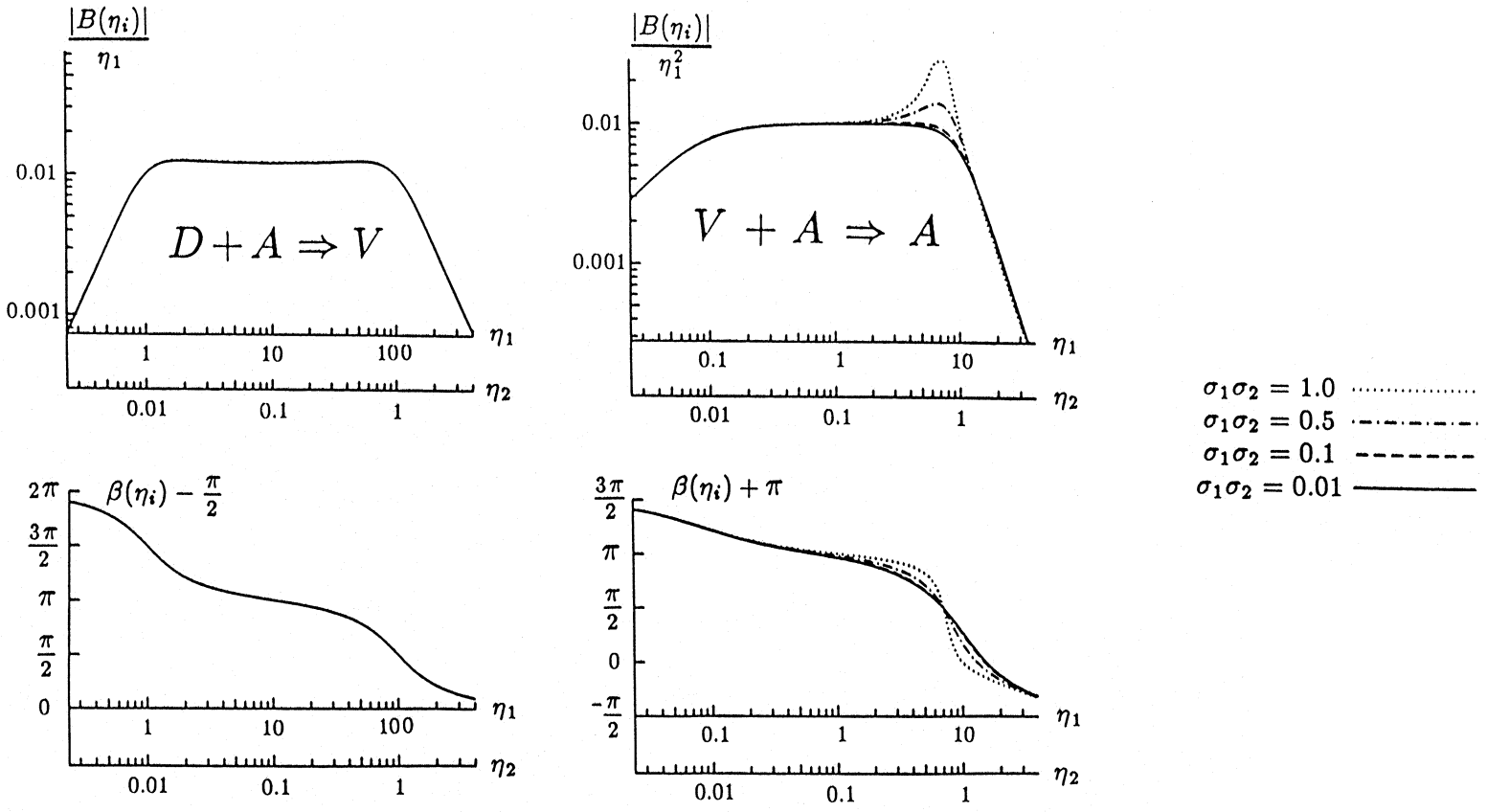

Fig. 2c Transfer function of a coupled transducer–galvanometer system. Case when "galvanometer measures acceleration" and left: "transducer measures displacement" ($D+A \Rightarrow V$), right: "transducer measures velocity" ($V+A \Rightarrow A$); see also the last row in Table 2. The transfer function $B(\eta_1, \eta_2)$ of the coupled system is plotted versus dimensionless frequencies η_1, η_2 for several values of σ_1, ($\sigma_2 = 1$). The critical damping ratios are assumed to be 6.0 for velocity-type device and 0.6 for displacement and acceleration-type devices. The plots in the top of the figure show the normalized amplification, and in the second row show the phase shift of the measured quantity.

is better for the amplitude response (makes it more stable), and big coupling—for the phase response.

The above analysis and careful study of the Table 2 and Fig. 2 lead to the conclusion that the correction of the output of the coupled "transducer–galvanometer" system for instrument response is necessary for any value of coupling even in the frequency range where the amplitude response is stable, because of the phase distortion. Obviously, correction is also needed if we wish to increase the frequency range where the amplitude response of the system can be considered to be "flat".

III. CORRECTION FOR THE INSTRUMENT RESPONSE OF A COUPLED SYSTEM

The general scheme for the proposed method is based on Eq. (2) and can be presented by the flow chart of Fig. 3.

Before applying the numerical procedures, shown in Fig. 3, the frequency band of interest should be identified. This can be done by comparison of the Fourier spectrum of the direct output from the system with the average noise spectrum for a typical record. By "noise" here we mean mostly digitization noise (Amini et al., 1987; Lee et al., 1982; Trifunac et al., 1973), and consider the other distortions of the signal to be the part of a signal itself. Having Fourier spectra for both noise and the signal with noise, one can determine the upper (f_1) and the lower (f_2) limits of the frequency band for any desired signal to noise ratio. It is customary to work whithin frequency band where this ratio is greater or equal to one, so that no information is lost.

Each differentiation and integration from the flow chart in Fig. 3 should be accompanied by low- or high-pass filtering with low cut-off f_2 and high cut-off f_1. This is necessary because differentiation emphasizes high frequencies (higher than f_1) which do not have any useful information, and integration does the same with low frequencies (lower than f_2). So, low-pass, high-pass, differentiation and integration filters are all required. We will see later on that an interpolation procedure is also necessary.

III.1. Digital Filters Used in the Process

We will describe now the filters used in this work. Each circle in Fig. 3 may represent application of a sequence of filters. For example, differentiation is always accompanied by low pass filtering and integration requires both low- and high-pass filters.

III.1.1. Differentiation

The pulse response of the differentiating filter can be represented by

$$w_{\pm k} = \frac{\pm 1}{k} \cdot \left\{ \frac{\sin(\pi k/N)}{(\pi k/N)} \right\}^2, \quad w_0 = 0, \; k = \overline{1, N}. \tag{20}$$

Here w_k designates the weights of the filter, the overline in $k = \overline{1, N}$ means that k varies from 1 to N, so that $2N + 1$ is equal to the total number of points in the filter. Factor $\{\cdot\}^2$ represents squared Lanczos coefficients which are introduced to reduce the Gibb's phenomenon (Hamming, 1983). The antisymmetry of the filter provides for the "exact" behavior of the phase (it is not distorted with respect to the theoretical $\frac{\pi}{2}$ value).

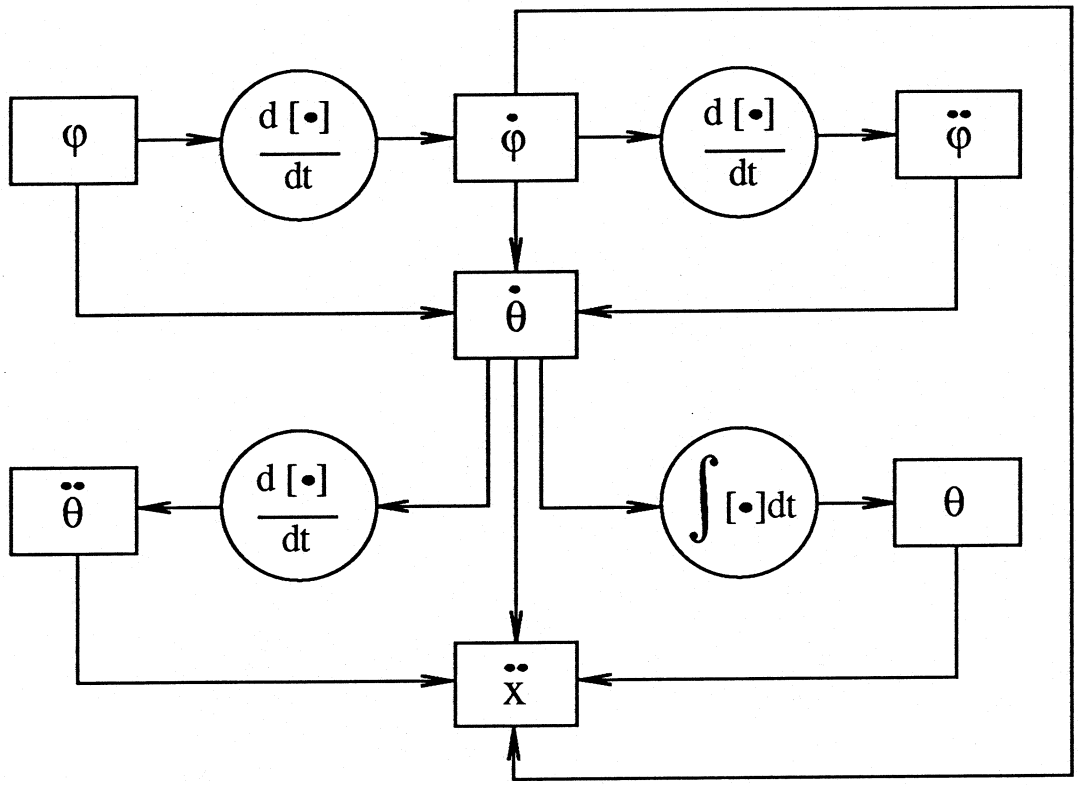

Fig. 3 General scheme of the instrument correction procedure for the coupled 2DOF system, represented by Eq. (2). Having the response of the system φ one can get $\dot{\varphi}$ and $\ddot{\varphi}$ by two numerical differentiations. Knowing all the constants involved in Eq. (2b), the first derivative of the transducer response $\dot{\theta}$ can be obtained. Further, numerical differentiation and integration gives $\ddot{\theta}$ and θ. The last step is to compute $\ddot{x}$ from Eq. (2a) with known $\theta, \dot{\theta}, \ddot{\theta}$ and $\dot{\varphi}$.

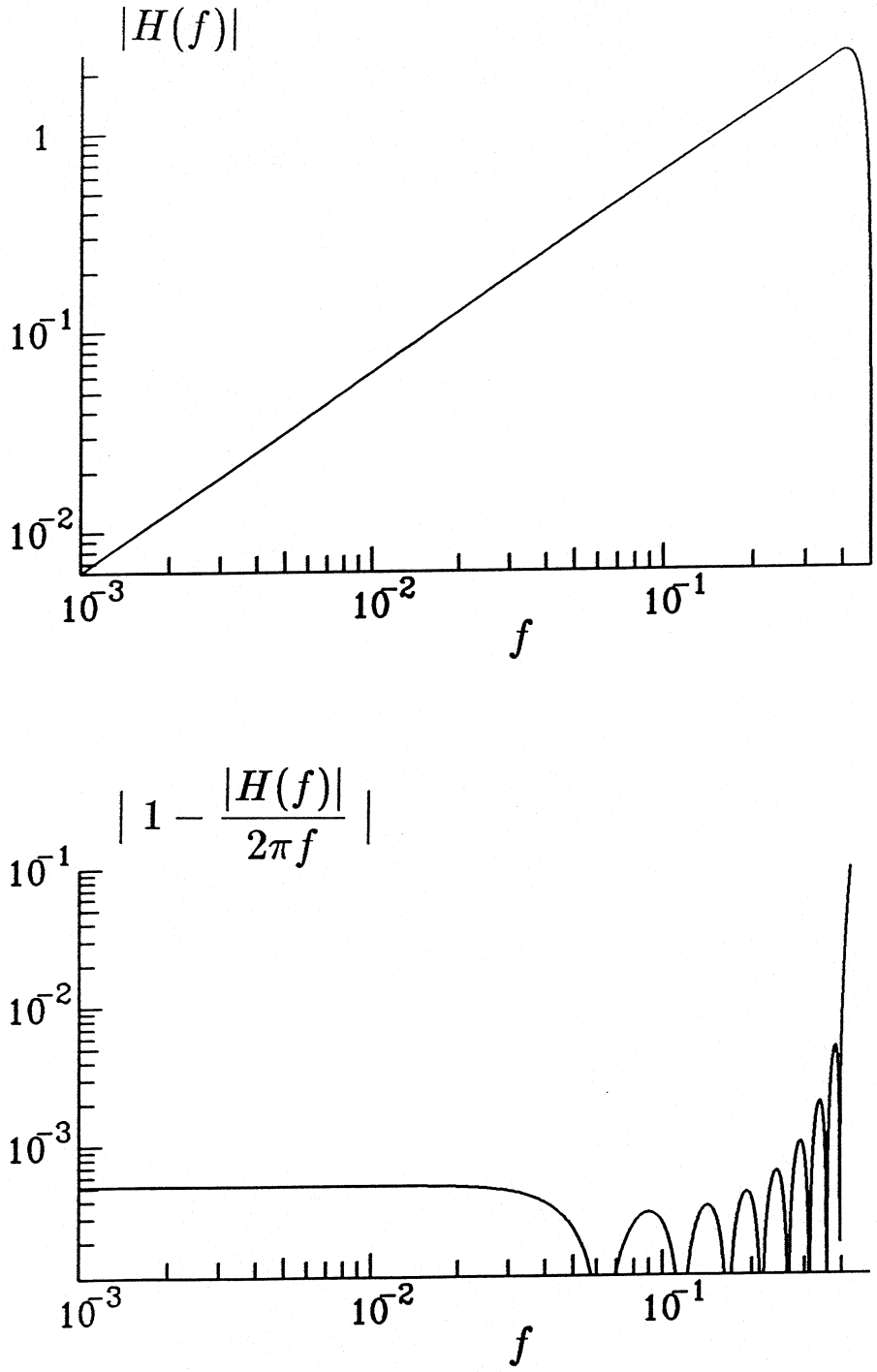

Fig. 4 The moduli of the transfer function of the numerical differentiator, used in the instrument correction procedure (top) and its relative error (bottom). The total length of the filter is 21 points. The dimensionless frequency f (horizontal axis) is expressed in terms of the sampling frequency, so that the Nyquist frequency is equal to 0.5.

The modulus of the transfer function of this filter can be evaluated as:

$$|H(\omega)| = \Big| \sum_{k=1}^{N} 2 \cdot \mathrm{w_k} \cdot \sin \omega \mathrm{k} \Big| . \tag{21}$$

The transfer function in Eq. (21) of the filter in Eq. (20) with $N = 10$ is shown in Fig. 4 (top). As the transfer function of the differentiation should ideally be proportional to ω, the quantity $\{1 - |H(\omega)|/\omega\}$ describes the relative error of the numerical differentiation (Fig. 4 bottom). As it can be seen from the figure, the accuracy of this filter is 10^{-3} for $f < 0.31$ and 10^{-2} for $f < 0.4$. The frequency, f, is expressed in terms of the sampling frequency, so that the meaningful range of f is from zero to 0.5, where $f = 0.5$ is the Nyquist frequency, which is the highest one that can be resolved by a sampling rate. It is useful to recognize that during the actual numerical differentiation, small error, predicted by the above transfer function (Eq. (21) and Fig. 4), can be achieved only if the process is infinitely long and stationary. The beginning and the end of a record will be distorted (with respect to whatever is predicted by the transfer function) by any filter. Difficulties associated with the record extension beyond the actually recorded time can be avoided in the case of continuous recording.

III.1.2 Integration

The symmetrical 3 point IIR Chebyshev filter (Hamming, 1983) was chosen as an integrator. This filter is defined by

$$y_{n+1} = y_{n-1} + a y'_{n+1} + b y'_n + a y'_{n-1},$$

where y'_n stands for the input function, y_n is the output from the integrator, and a and b are coefficients to be determined by two conditions. First, $y'(t) =$ const., should be integrated exactly. This gives

$$2 = 2a + b. \tag{22}$$

Second, the error curve at any frequency is to be a Chebyshev function in the lower λ part of the Nyquist interval (that is, from 0 up to $\lambda \cdot 0.5$ in terms of sampling frequency). This gives the second equation:

$$2\pi\lambda a J'_1(\pi\lambda) + \pi\lambda b J'_1(0) = 2J_1(\pi\lambda), \tag{23}$$

where $J_1(x)$ is the Bessel's function of order one and with argument x. The symmetry of the filter allows one to avoid the phase errors. Solution of Eq. (22) and Eq. (23) gives the constants a and b for any $0 \leq \lambda \leq 1$. The modulus of the transfer function of this integrator can be represented as

$$|H(\omega)| = \Big| \frac{2a \cos\omega + b}{2 \sin\omega} \Big|, \tag{24}$$

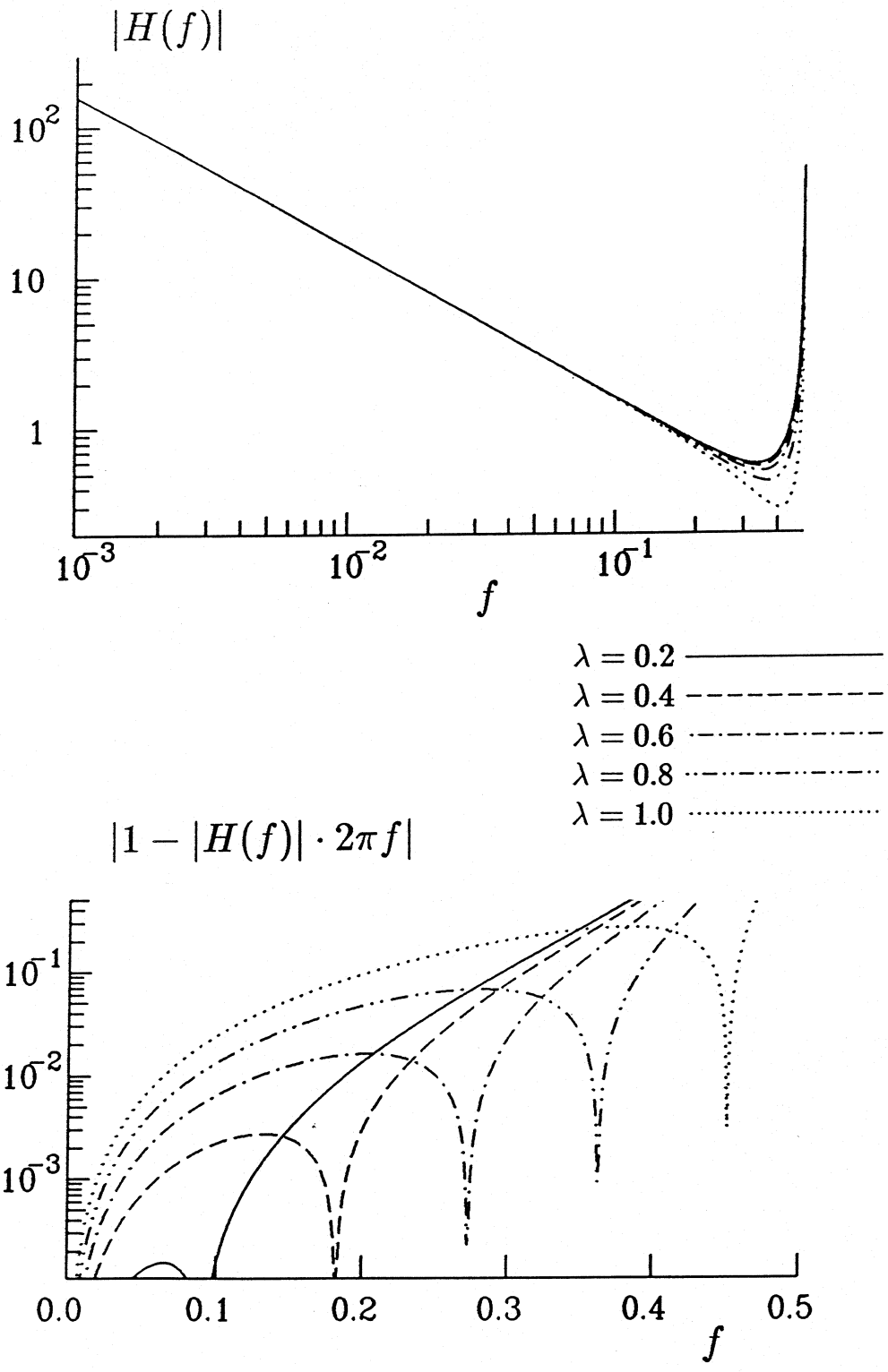

Fig. 5 The moduli of the transfer function (top) and of the relative error of the integration procedure (bottom) for 3 points Chebyshev integrator. λ designates the part of the Nyquist interval were the error is kept as small as possible. The dimensionless frequency f is expressed in terms of the sampling frequency.

and the error is described by $\{1-|H(\omega)|\cdot\omega\}$. Plots of the transfer function Eq. (24) and of the error are presented in Fig. 5. Notice that it is not practical to require high frequencies to be integrated precisely with this type of filter. In general, it is not recommended to take $\lambda > 0.5$.

To start the integration, the initial conditions should be known. Lack of this information forces one to assume zero initial conditions and, after integration is accomplished, to "correct" the result. This correction takes care also of a possible linear drift due to non ideal position of a zero line in the input function and is just a subtraction of the least-square straight line from the result obtained by the integration of the input function.

III.1.3. Low-Pass Filter. High-Pass Filter with "Not Very Low" Cut-off Frequency

Two types of filters were considered for the purpose of low- and high-pass filtering.

The symmetrical pulse response of the low-pass version of the first one was chosen to be

$$\mathrm{w}_{\pm k} = \frac{1}{\pi k}(\sin(2\pi f_1 k)) \cdot \mathrm{w}_k^*, \quad \mathrm{w}_0 = 2f_1, \quad k = \overline{1, N}, \tag{25}$$

where w_k are the filter weights and f_1 is the low cut-off frequency. The last term w_k^* represents the Webber's windowing, which can be approximated by two cubic parabolae (Cappellini et al., 1978).

The high-pass version of this filter can be represented by

$$\mathrm{w}_{\pm k} = \frac{1}{\pi k}(\sin \pi k - \sin 2\pi f_2 k) \cdot \mathrm{w}_k^*, \quad \mathrm{w}_0 = 1 - 2f_2, \; k = \overline{1, N} \tag{26}$$

where f_2 is the high cut-off.

The required length of the filter $N_{tot} = 2N + 1$ can be estimated by the empirical formula $N_{tot} \approx 2/f^*$, where f^* is the narrowest frequency interval for which the amplitude response of the filter can be realized. Suppose we want to have a sharp filter, so that the transition band is much smaller than the cut-off frequency f_c (which is equal to f_1 or f_2). In that case, f^* can be considered to be equal to the width of the transition band, which may be taken as, say $f_c/10$. This gives us the estimation of the required filter length as

$$N_{tot} \approx \frac{20}{f_c}. \tag{27}$$

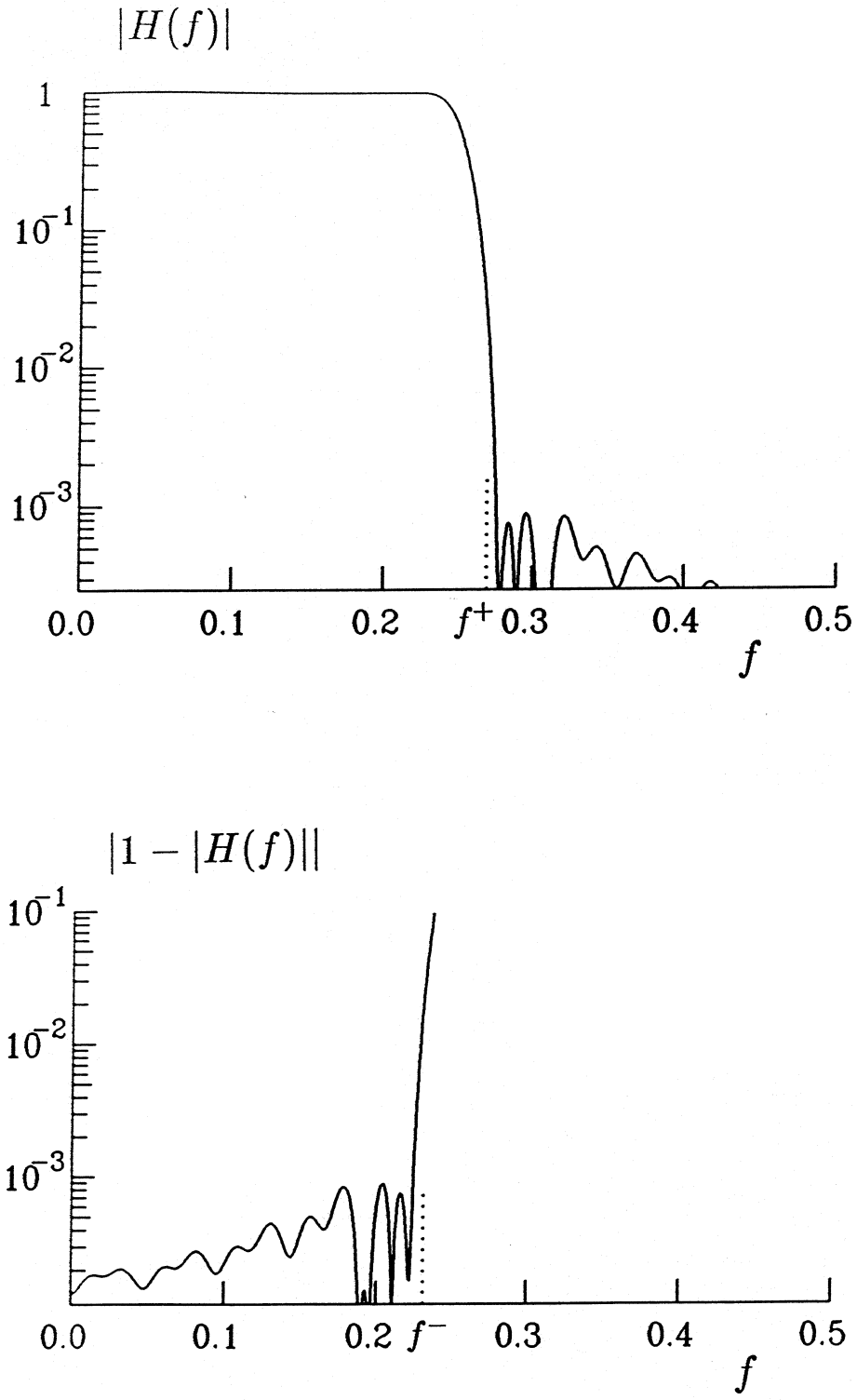

Fig. 6 A "sharp" filter amplitude transfer function (top) and the corresponding error (bottom). The transition band lies between frequencies f^- and f^+, and $f_1 = 0.25$ (in terms of the sampling frequency). The half-length $N = 40$ (the total number of points is 81).

The modulus of the transfer function of any symmetrical (preserving zero phase) filter can be written as

$$|H(\omega)| = \Big| \sum_{k=1}^{N} 2 \cdot \mathrm{w_k} \cos(\omega \mathrm{k}) + \mathrm{w_0} \Big| . \tag{28}$$

Fig. 6 (top) represents $|H(\omega)|$ in Eq. (28) for the low-pass filter in Eq. (25) with $f_1 = 0.25$ and $N = 40$. Fig. 6(bottom) shows the error of the filter. The transition band here is defined as the difference between the frequencies f^- and f^+, where f^- is the point were the error in the pass-band becomes greater than 10^{-2}, and f^+ is the point were the error in the stop-band becomes smaller than 10^{-2}. In the case presented $f^+ - f^- \approx 0.03$, so that $f^+ - f^- \approx f_1/10$ and the estimate of N_{tot} in Eq. (27) is reasonable. All the properties of the high-pass filter in Eq. (26) are like a mirror image of the properties of its low-pass counterpart Eq. (25).

The second type of filter is the Ormsby filter and it is used for high- and for low-pass filtering when $f_c < 0.25$. "Sharp" approach (i.e. small transition within the response of the filter, Eq. (25)–(27)) leads to unreasonable length of this filter for small f_c. The reduction of the number of the filter weights results in the poor control of the shape of the transition band. Ormsby low-pass filter with von Hann windowing

$$\mathrm{w}_{\pm k} = \frac{\cos(\omega_c k) - \cos(\omega_s k)}{2\pi^2(\omega_s - \omega_c)k^2} \cdot \left\{ \frac{1}{2} \left[1 + \cos\left(\frac{k\pi}{N} \right) \right] \right\}, \quad \mathrm{w_0} = \frac{\omega_s + \omega_c}{4\pi^2}, \quad k = \overline{1, N} \tag{29}$$

effectively reduces the width of the transition band for small corner frequency with respect to the "sharp" filter with the same N by providing better control of the slope between the ω_c (the cut-off frequency) and ω_s (the roll-off frequency). The number of weights in the filter can be estimated from

$$N_{tot} = 2N + 1 \approx \frac{4\pi}{\omega_s - \omega_c}. \tag{30}$$

For a reasonable balance between the length and the sharpness of the filter in Eq. (29), an empirical estimation of the relative width of the transition band can be considered (Fig. 7). The transfer function for a typical cut-off $f_1 = \omega_c/2\pi = 0.12$ (which corresponds to 24 Hz with 200 Hz sampling frequency) is presented in Fig. 8. The width of the transition band and the number of points in the filter were chosen in agreement with the empirical estimate illustrated in Fig. 7 and in Eq. (30).

If one needs to perform a high-pass filtering with the help of the filter in Eq. (29), this can be done in two steps. First, low-pass filtering with ω_c and ω_s exchanged (as compared with what is required by the ordinary one-step low-pass) has to be performed. Second, the result of the first operation has to be subtracted from the original time series. However, even for $(\omega_c - \omega_s)/\omega_c = 0.5$, the number of filter weights becomes very large if $f_c \lesssim 1/50$ (in terms of sampling frequency). Within digitization frequency of 200 Hz (which is common in seismological and earthquake engineering data processing), this corresponds to corner frequency $\approx$ 4Hz. Obviously, cut-off much lower than 4Hz is

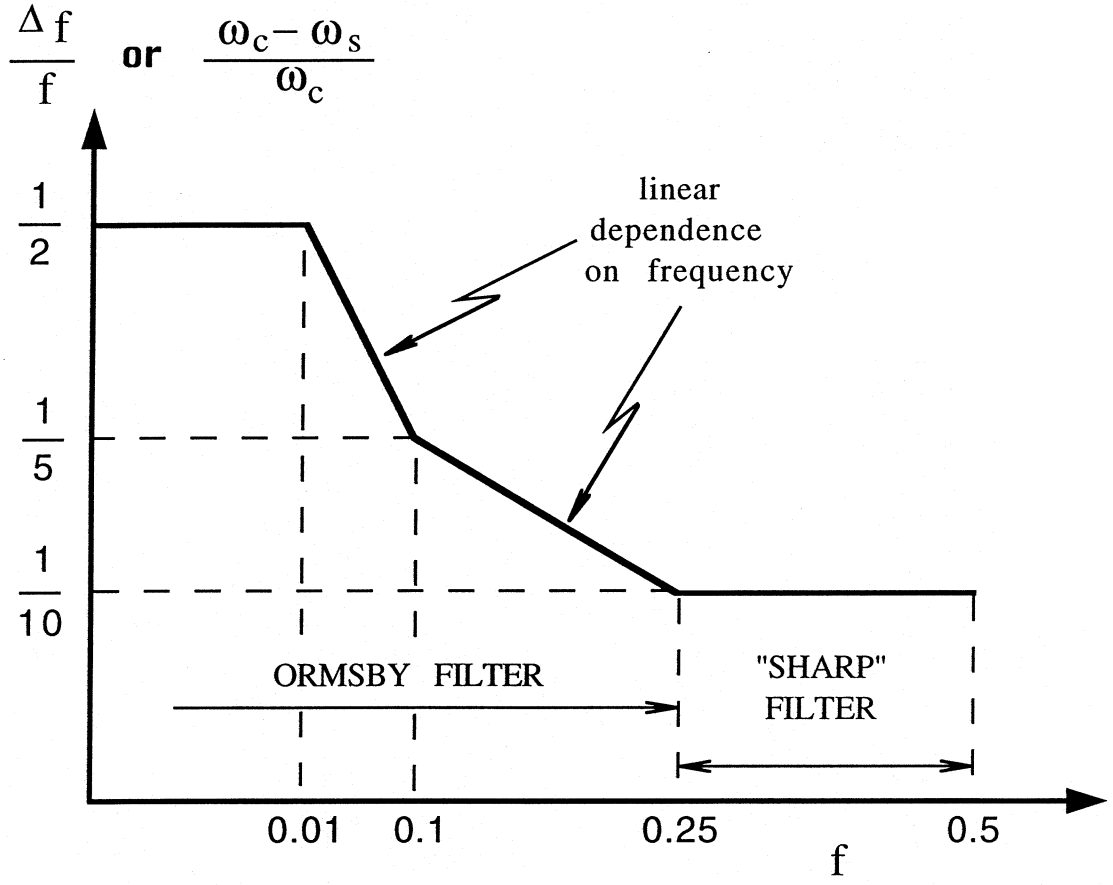

Fig. 7 Empirical relation between the corner frequency f_c(or ω_c) and the width of the transition band Δf (or $\omega_s - \omega_c$) for obtaining a "reasonable" length of the filter. The dimensionless frequency f is expressed in terms of the sampling frequency.

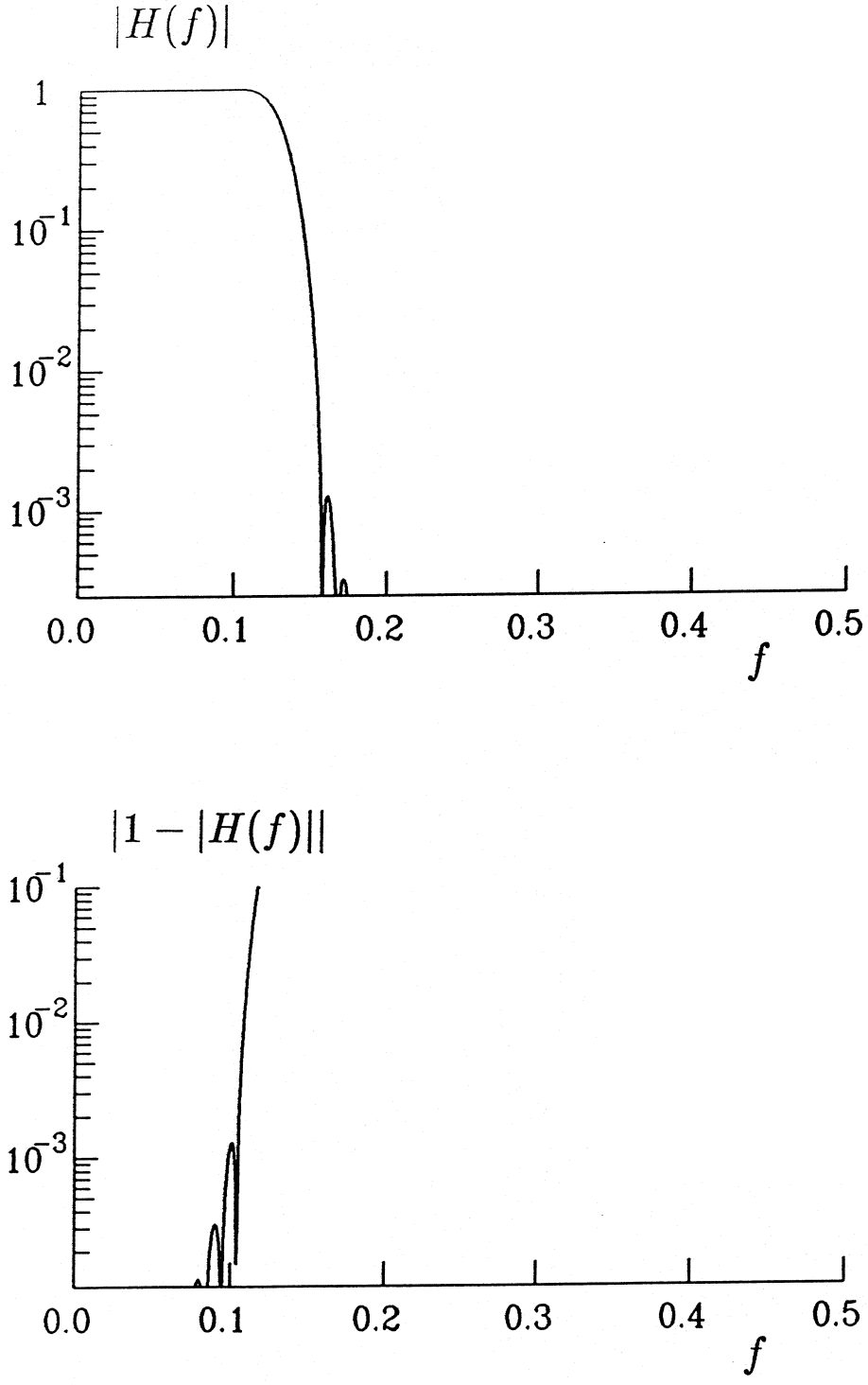

Fig. 8 Ormsby filter transfer function amplitude (top) and the corresponding error (bottom), for $f_1 = 0.12$. The other parameters were chosen according to Fig. 7 and Eq. (30) and are: $\Delta f = 0.022$ and $N = 44$ (the total number of points is 89). The dimensionless frequency f is expressed in terms of the sampling frequency.

required in the high-pass procedure for a great number of cases (f_2 is usually smaller than .5Hz). At the same time, large number of points in the filter results in slowing down of the computations and in accumulating numerical errors.

III.1.4. High-Pass Logic ("Very Low" Frequency Cut-off Case)

As we saw in the conclusion of the previous section, in the majority of cases the straightforward high-pass filtering is not practical, and the scheme presented in Fig. 9 can be considered.

The idea of the scheme in Fig. 9 is quite simple: if it is difficult to implement the straightforward high-pass filtering, the complementary low-pass procedure can be performed instead (this can be easier to do) and then the low-pass filtered result should be subtracted from the original signal. It appears to be easier to do low-pass filtering because the frequencies one wants to preserve are very low; so one does not need high sampling frequency to operate on the record. Thus, the idea of decimation comes in. Computer time is proportional to $n \cdot N$, where n is the length of the record in points, and $2N+1$ is the number of points in the filter. The decimation reduces both n and N several times. A variety of schemes for high-pass filtering with decimation and backward interpolation are available (Crochiere and Lawrence, 1975; Oetken et al., 1975; Shively, 1975; Mintzer and Liu, 1978, to mention just a few). The method presented here was chosen because of its simplicity.

We next discuss each step in Fig. 9 in some detail.

Step #1. Preliminary low-pass filtering is necessary to make the decimation possible. Due to the phenomenon of aliasing, it is necessary to have $f_{\text{highest}} < Ny^{\text{new}}$ during the decimation process. Here f_{highest} designates the highest frequency that is present in the record at the time of decimation and Ny^{new} is the new Nyquist frequency—the one that we want to decimate the record to. Thus, before decimation, one should filter out all frequencies that are higher than Ny^{new}. What should be the properties of this preliminary low-pass (pre-low-pass) filtering? It should filter out all $f > Ny^{\text{new}}$, not disturbing all frequencies $f < f_2$, where f_2 is the cut-off of the initial operation to be to accomplished (high-pass). To perform preliminary low-pass, we choose Ormsby filter with $(\omega_s - \omega_c)/\omega_c = 1$, so that (to play it safe) all frequencies $\omega > 4\omega_c$ will be definitely filtered out. In other words, the requirement for the pre-low-pass filtering is

$$\rho = \frac{Ny^{\text{new}}}{f_1^{\text{pre}}} \geq 4, \tag{31}$$

where f_1^{pre} designates the cut-off frequency of the filter, i.e. $2\pi f_1^{\text{pre}} = \omega_c$. We will see later that the "safety factor" of 4 is necessary for some other reason.

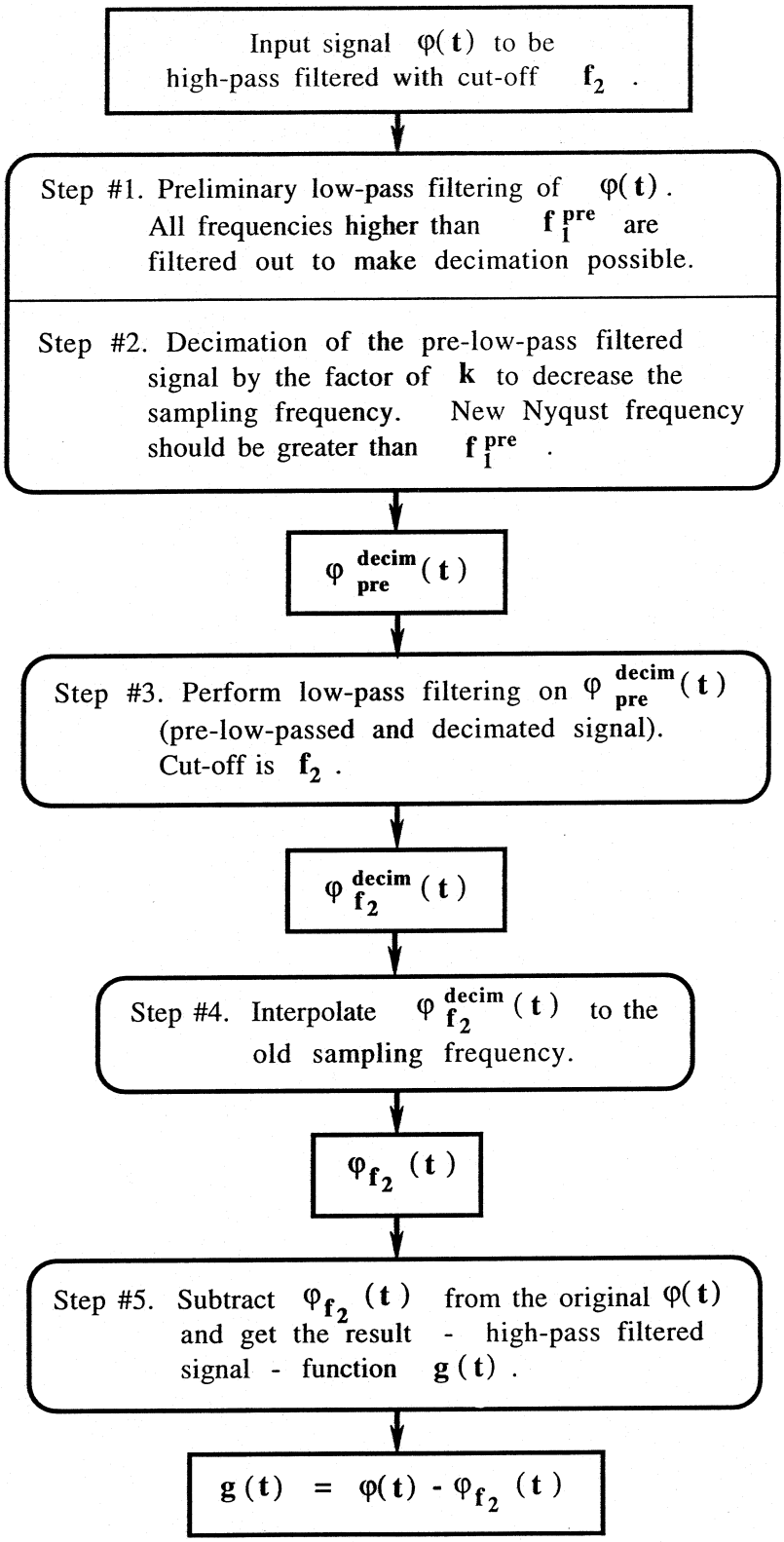

Fig. 9 Flow chart of the high-pass filtering procedure for the case of "very low" cut-off frequency f_2.

The filter length $2N^{\text{pre}}+1$ required can be estimated from Eq. (30) or, in terms of the pre-low-pass cut-off:

$$N^{\text{pre}} = \frac{1}{f_1^{\text{pre}}}. \tag{32}$$

Step #2. After preliminary low-pass filtering the record is ready to be decimated. Designating the factor of the decimation by k, the following results,

$$Ny^{\text{new}} \cdot k = Ny^{\text{old}} = 0.5, \qquad k \geq 2 \tag{33}$$

Here Ny^{old} is the initial Nyquist frequency, which is equal to the half of the sampling frequency. However, it is not practical to perform Steps #1 and #2 separately. Actually, during the pre-low-pass filtering, only every k^{th} point should be calculated, and this saves computer time considerably making the whole procedure very efficient.

Step #3. This step performs low-pass filtering with corner frequency f_2 (in terms of the original cycle frequency). To avoid disturbance of the frequencies lower than f_2, one should have $f_1^{\text{pre}} \gg f_2$, because only very low frequencies were not disturbed at all by pre-low-pass filter (see later Fig. 12). Assuming that factor 4 is sufficient, one can write

$$\rho' f_2 < f_1^{\text{pre}}, \qquad \rho' \geq 4. \tag{34}$$

Notice, that decimation reduces the length of the record and of the filter in terms of points, but this does not affect the physical length of either of them. Hence, the length of the Ormsby filter, estimated with the help of Fig. 7 and Eq. (30), can still be much greater than the length of the record is. At this point one can introduce an additional constraint

$$N_{tot} < 1.8n, \tag{35}$$

where N_{tot} and n are the length of the filter and the length of the record respectively. The factor 1.8 does not have any specific physical meaning and comes from experience. The idea is that having the filter much longer than the record is not meaningful and filtering under such conditions will only introduce additional errors (recalling the fact that the filtered result "feels" the disturbance coming from the beginning and the end of the record during the time equivalent to the half of the length of the filter).

Step #4. Suppose one has low-pass filtered the record (up to f_2) with the new sampling frequency. Now we have to interpolate back to the old digitization frequency. The method used is the spline interpolation (Press et al., 1986) which can be tested as follows. We take

$$y_0(i) = \sin\left(\frac{2\pi}{\rho_1}(j-1)\right), \qquad j = \overline{1,n}$$

as an input function, where ρ_1 designates the number of points per period of the function (the bigger ρ_1 is, the smaller the error of interpolation becomes). During the interpolation procedure, the sampling rate increases k times as $k-1$ additional points are introduced inbetween every pair of initially defined points. Let us designate the output of the interpolation as $\tilde{y}(i)$ defined at all $i = \overline{1,l}$, where $l = k(n-1)+1$. The function, characterizing the error of the interpolation can be written as

$$q(i) = \tilde{y}(i) - \tilde{y}_0(i), \quad i = \overline{1,l},$$

where $\tilde{y}_0(i)$ is the initial function y_0 defined with k times increased sampling rate:

$$\tilde{y}_0(i) = \sin\left(\frac{2\pi}{\rho_1 k}(i-1)\right), \quad i = \overline{1,l}.$$

Define the error of the interpolation for this specific value of ρ_1 as:

$$\max_i |q(i)|.$$

Changing ρ_1, one can estimate the error of the interpolation, ϵ, as a function of the value of the highest frequency which is present in the record ($\rho_1 \approx 1/f_{\text{highest}}$), as

$$\epsilon(\rho_1) = \max_i |\tilde{y}(i) - \tilde{y}_0(i)|. \tag{36}$$

The parameter k in the logic presented describes the relative density of points where the initial function was defined. The graph of Eq. (36) for $k = 10$ is given in Fig. 10. Experiments show that the accuracy of the interpolation does not depend on k for $k \geq \rho_1$.

Next we summarize all conditions, given by Eq. (31)–(34) in Fig. 11. As it can be seen from this figure, the highest frequency that can be present in the record at the time of the interpolation, corresponds to at least $\rho'\rho$ points per period, and as $\rho \geq 4$ and $\rho' \geq 4$, this number is not less than 16. Going back to Fig. 10, the estimation of the interpolation error can be obtained for $\rho_1 \geq 16$. This error is $\leq 10^{-3}$, and that gives the answer to the question why a safety factor of 4 was chosen in the discussion on the pre-low-pass filtering procedure.

Step #5. Subtraction of the interpolated time series from the original function gives the desired result: high-pass filtered signal.

Further consideration of restrictions, summarized in Fig. 11, leads to the following conclusions. The flow chart in Fig. 9 can be used to perform high-pass filtering only if $f_2 < 0.5/(4^2 \cdot 0.2) = 1/64$. If this is so, one has to choose k, ρ and ρ'. This can be done

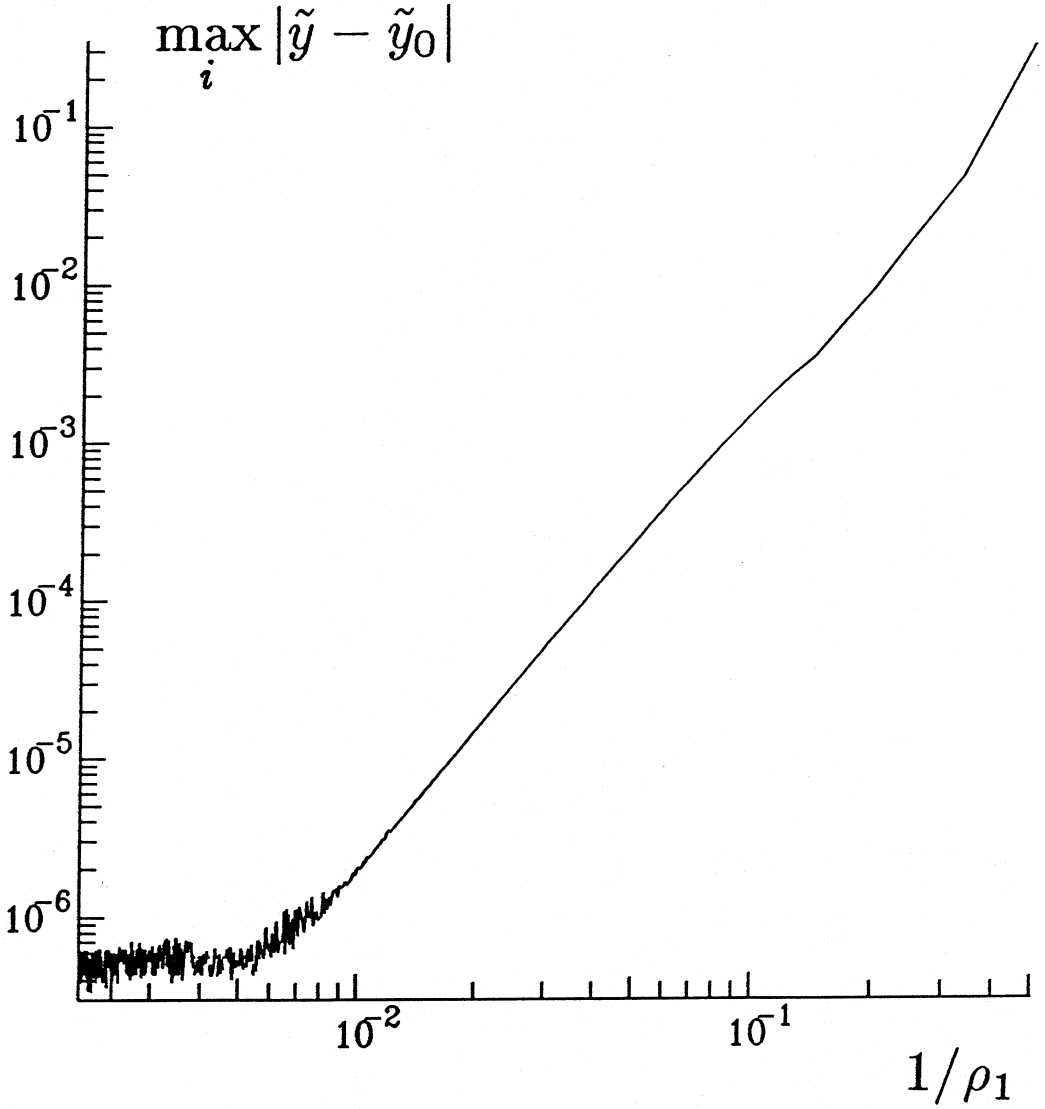

Fig. 10 Estimation of the error of the spline interpolation as a function of the number of points per period $(1/\rho_1)$ where the interpolated function is defined.

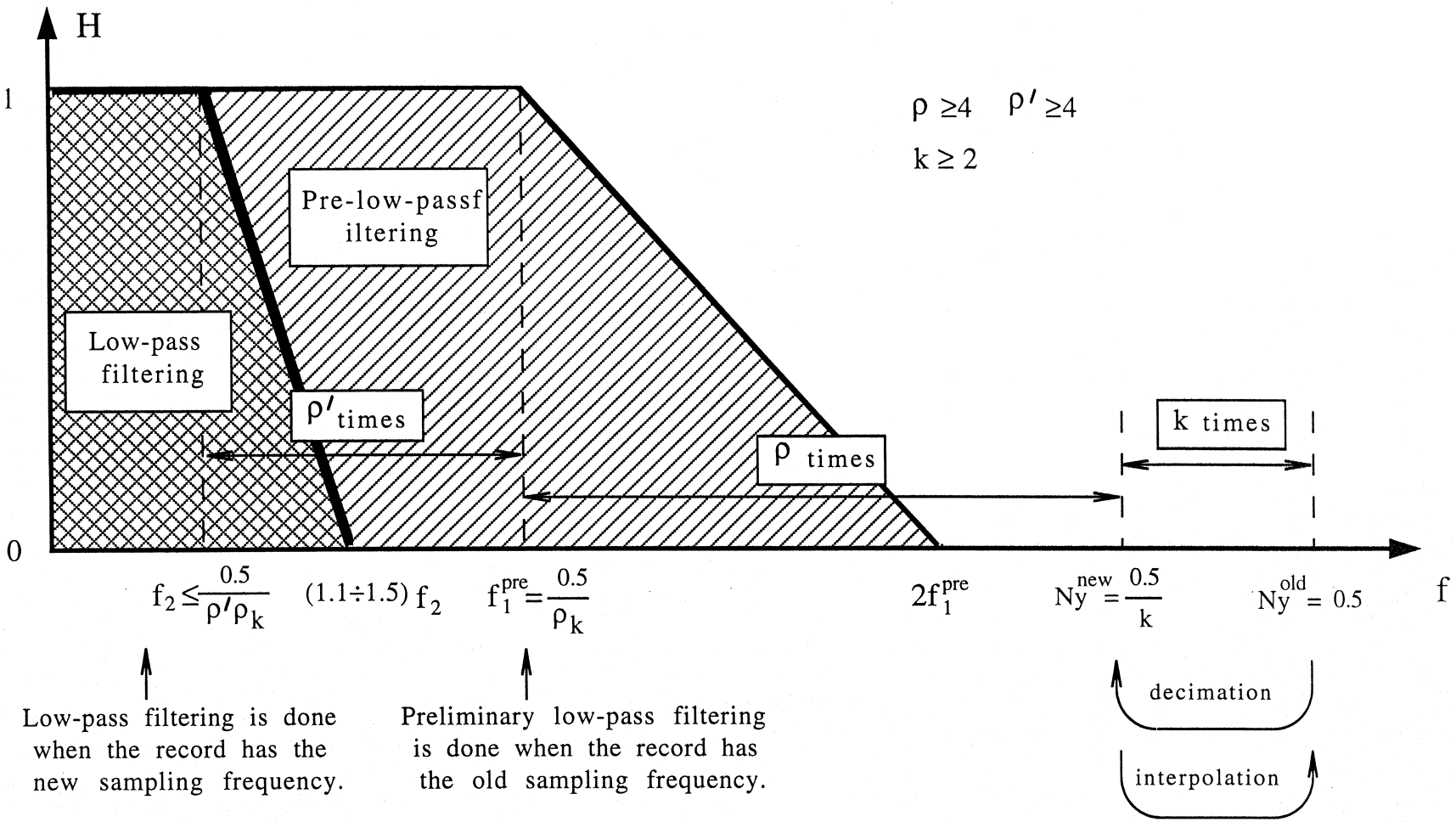

Fig. 11 Relationships among parameters involved in the logic of the high pass filtering with decimation.

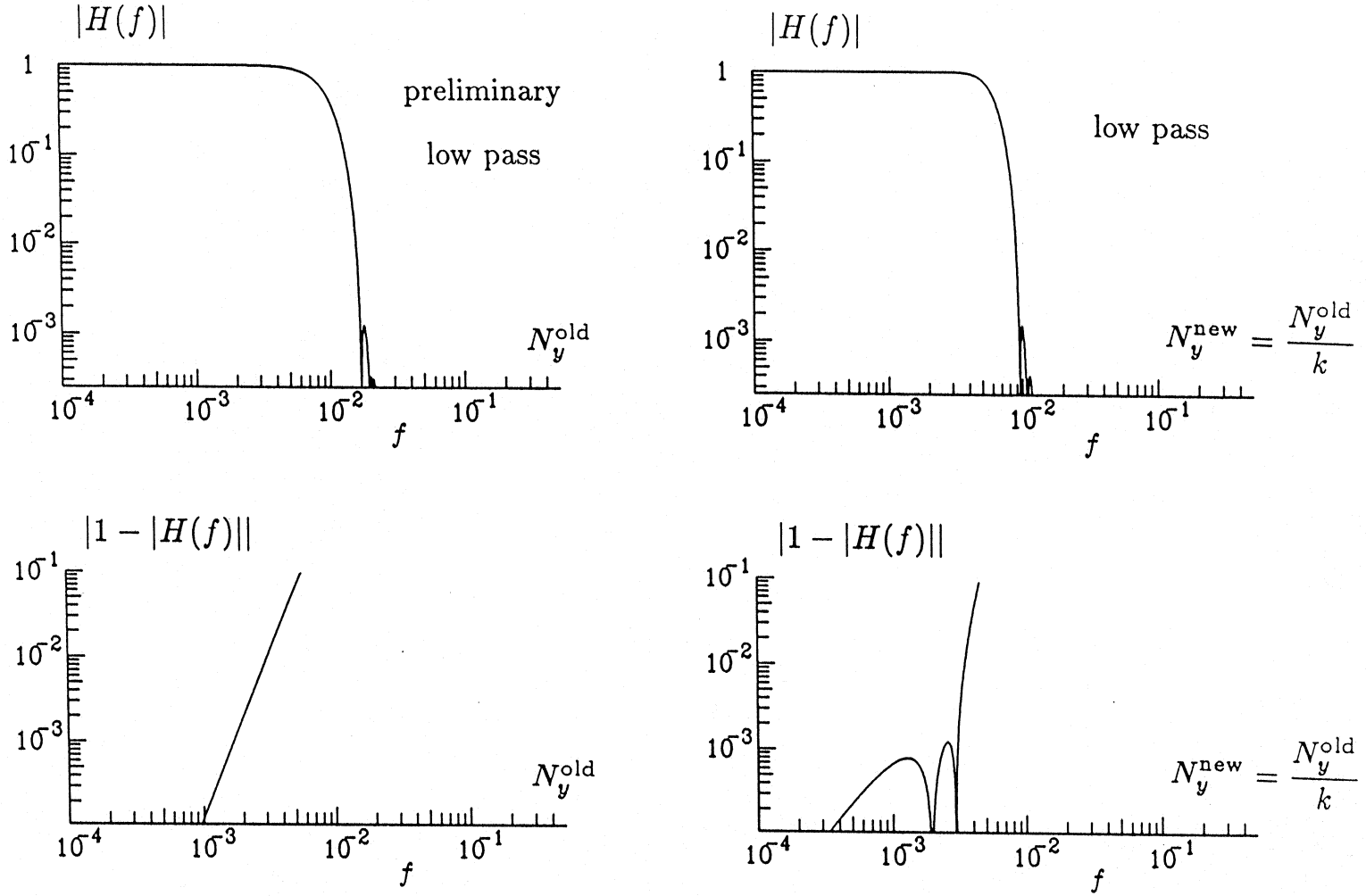

Fig. 12 Moduli of the transfer functions (top) and their errors (bottom) of the preliminary low-pass filter (left) and the low-pass filter (right) operations from the high-pass filtering algorithm. Given $f_2 = 0.0005$ (i.e. 0.05 Hz for 200 Hz sampling rate), the algorithm chooses $f_1^{\text{pre}} = 0.00625$, $N^{\text{pre}} = 160$, $\rho = 10$, $k = 20$ and $N = 342$ (according to Eq. (37)). Notice that the left graph is presented in terms of the sampling frequency before decimation ($Ny^{\text{old}} = 100$ Hz), while the right one has new sampling frequency ($Ny^{\text{new}} = 10$ Hz). In both cases dimensionless Nyquist frequency is 0.5.

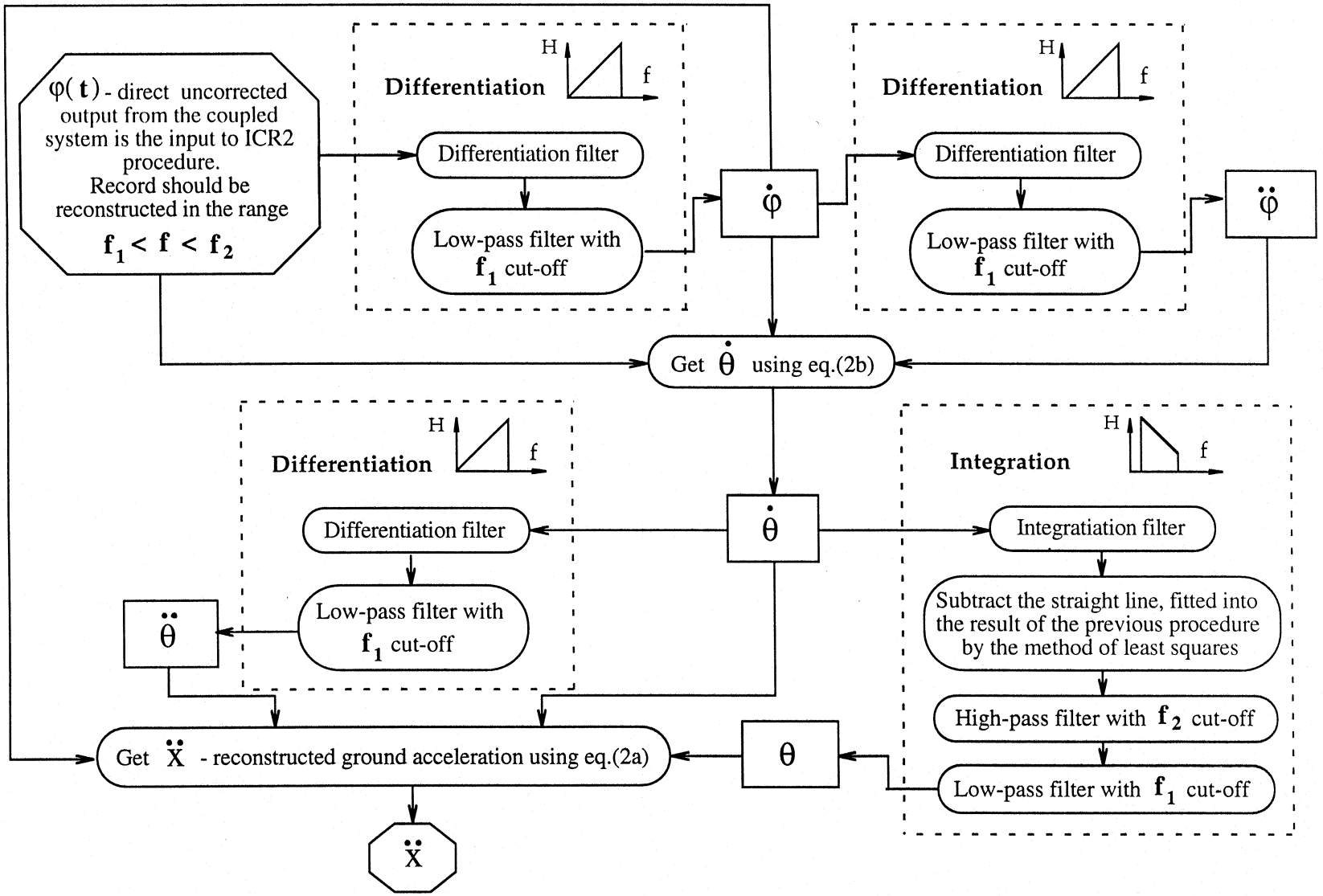

Fig. 13 Flow chart of the ICR2 procedures.

by minimizing the computer time necessary for the whole process and by taking advantage of the results obtained during the testing procedure. That leads to the following assumptions and estimates:

$$\begin{aligned} \rho' &= \rho \\ \rho &= \max\left(4, \frac{1}{\sqrt[3]{4f_2}}\right), \quad k = 2\rho \\ N^{\text{pre}} &= \min\left(\frac{1}{0.5/4k} = 8k, \quad 0.9n\right), \\ f_1^{\text{pre}} &= \frac{1}{8k}, \\ N &= \min\left(\frac{1}{\Delta f_2} \cdot \frac{1}{k}, \quad 0.9\frac{n}{k}\right), \end{aligned} \tag{37}$$

where Δf_2 is obtained in accordance with Fig. 7 for $f = f_2$.

Fig. 12 presents the transfer functions of the preliminary low-pass filter (Step #1 above) and of the low-pass filter (Step #3) for the given $f_2 = 0.00025$ (this is 0.05 Hz for 200 Hz sampling frequency). Parameters $\rho = 10$, k, N^{pre} and N were chosen according to Eq. (37). Preliminary low-pass is done with 200 Hz sampling frequency (i.e. $N_y^{\text{old}} = 100$ Hz) by convolution with Ormsby filter with $N^{\text{pre}} = 160$, corner dimensionless frequency $f_1^{\text{pre}} = 0.00625$ (1.25 Hz in 200 Hz sampling frequency) and with the width of the filter equal to its corner frequency (i.e. $(\omega_s - \omega_c)/\omega_c = 1$). After decimation (during filtering only every k^{th} point was calculated) with factor $k = 20$, the record has 10 Hz sampling frequency and, therefore, new Nyquist frequency $Ny^{\text{new}} = Ny^{\text{old}}/k = 5$ Hz. Now, f_2 is equal to 0.005 (the same 0.05 Hz, but now for a 10 Hz sampling). Main low-pass is nothing else but convolution with Ormsby filter with corner $f_2 = 0.005$, $\Delta f_2 = f_2/2$ (see Fig. 7) and half-length $N = 342$.

III.2. The flow of the program ICR2

Using the filters discussed in Section III.1, the program ICR2 (Instrument Correction for the Response of a two degree of freedom coupled system) was written. Fig. 13 presents the flow chart of the logic of this program.

The output of the procedure is supposed to represent the reconstructed ground acceleration. If velocity or displacement are the quantities of interest, additional integrations should be performed.

The testing shows that the time necessary to reconstruct one record of about 50 sec duration with 200 Hz sampling frequency and the low cut-off at 10 sec and high cur-off at 25 Hz, is about 2 minutes on IBM-PC-AT with a DEFINICON accelerator board. The most critical quantities here are the value of the high cut-off expressed in terms

of the sampling frequency (this determines the length of the filters in low-pass filtering which is done 4 times in the program) and the length of the record (number of points). The lower the cut-off is and the longer the record is, more time is necessary to perform the instrument correction.

III.3 The Transfer Function of the ICR2 Procedure

The ICR2 was designed to perform the correction of the record for the instrument response. One way to check the quality of the algorithm is to get it's transfer function. Given the (generally) coupled device with known characteristics, the transfer function $B(\omega)$ is known (see Eq. (5)). The relationship between the input (displacement of the moving point $x(\omega)$) and the output (rotational response of the galvanometer $\varphi(\omega)$) can be expressed as

$$B(\omega) \cdot x(\omega) = \varphi(\omega)$$

in the frequency domain. Therefore, the acceleration of the moving point $\ddot{x}(\omega)$ can be obtained as

$$\ddot{x}(\omega) = -\omega^2 [B(\omega)]^{-1} \cdot \varphi(\omega). \tag{38}$$

The ideal instrument correction procedure should be able to reconstruct $\ddot{x}(\omega)$ inside prescribed frequency band $f_2 < f < f_1$. From this point, we will change our notation, and will express frequency in Hertz, and not as a dimensionless quantity scaled in terms of the sampling frequency. Designating the transfer function of ICR2 as $R(\omega)$, we have

$$\ddot{x}(\omega) = R(\omega) \cdot \varphi(\omega). \tag{39}$$

The accuracy of the instrument correction can be measured as the discrepancy between the theoretical Eq. (38) and actual Eq. (39) transfer function. The relative error is given by

$$\varepsilon(\omega) = \frac{-\omega^2 [B(\omega)]^{-1} - R(\omega)}{-\omega^2 [B(\omega)]^{-1}} \tag{40}$$

However, direct implementation of Eq. (40) is impossible as the analytical expression for $R(\omega)$ is not known.

To evaluate $|\varepsilon(\omega)|$ the following test was performed. Given harmonic input $\varphi_\omega(t) = \sin \omega t$, both actual $\ddot{x}_\omega(t) = r_\omega[\sin(\omega t + \beta(\omega))]$ and theoretical $\ddot{x}^0_\omega(t) = b_\omega[\sin(\omega t + \beta^0(\omega))]$ responses of the instrument correction algorithm can be obtained: the former by just running the ICR2 program, and the later analytically. As all the filters involved are symmetrical (or antisymmetrical), one can assume that the instrument correction procedure reconstructs the phase perfectly ($\beta(\omega) = \beta^0(\omega)$). This allows one to estimate r_ω / b_ω as the discrepancy between $\ddot{x}_\omega(t)$ and $\ddot{x}^0_\omega(t)$ at their (say) maxima. Carrying out calculations for a wide range of frequencies, the estimate of the relative error of the instrument correction procedure can be obtained:

$$|\varepsilon(\omega)| = \frac{b_\omega - r_\omega}{b_\omega} = 1 - \frac{r_\omega}{b_\omega}. \tag{41}$$

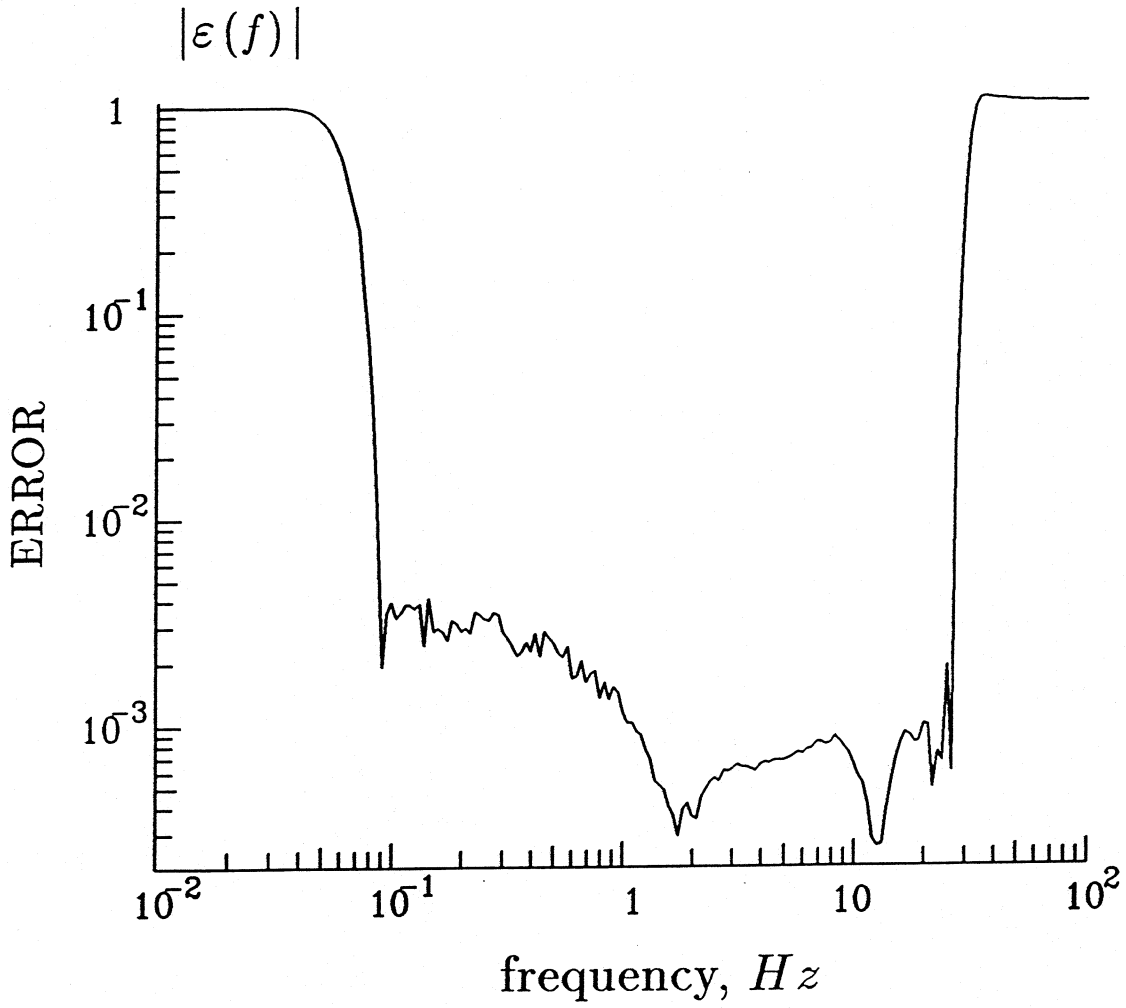

Fig. 14 Relative error of the ICR2 procedure in the case of a harmonic input.

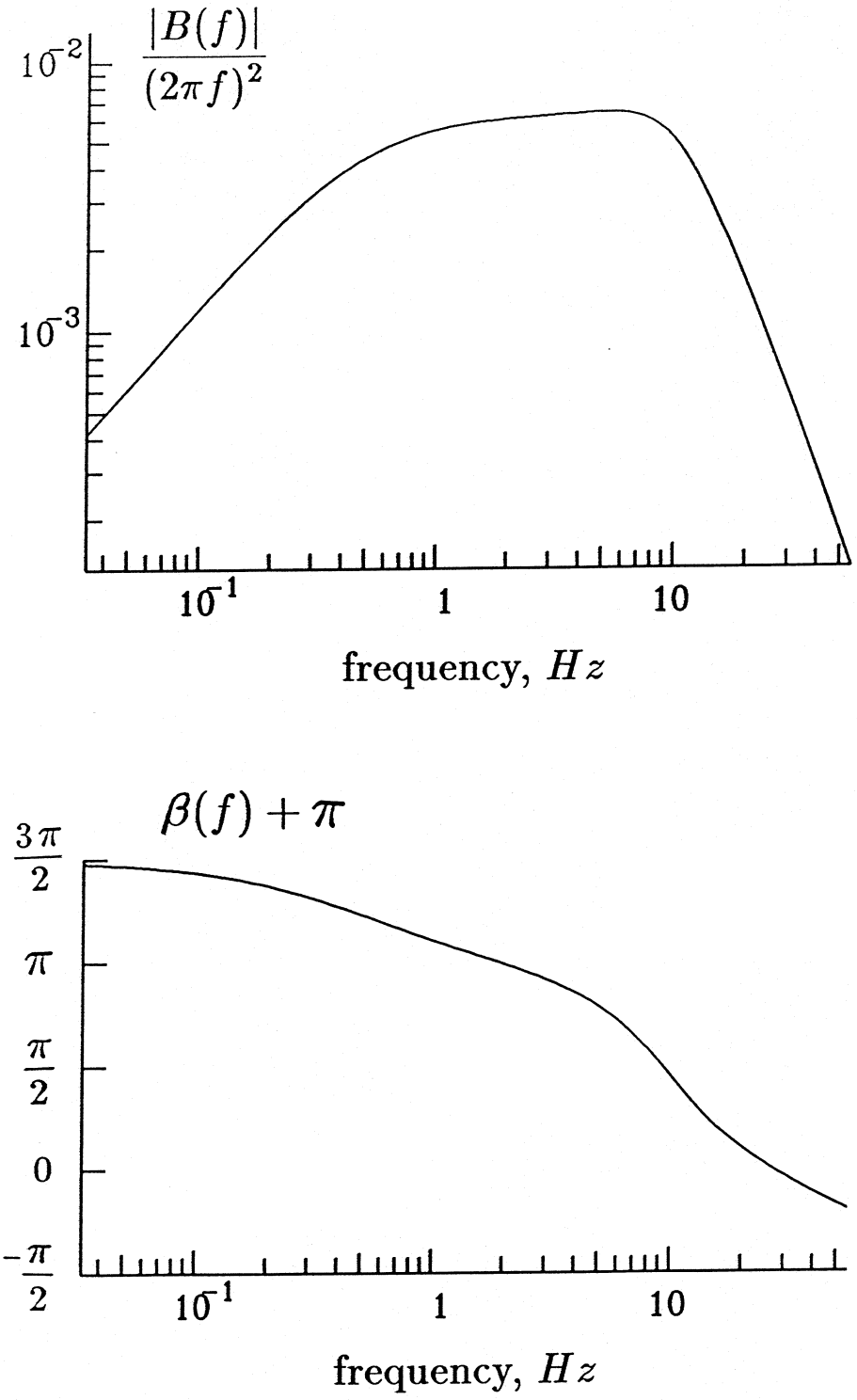

Fig. 15 The amplitude (top) and the phase (bottom) of the transfer function for the device $V + A \Rightarrow A$ with parameters: transducer's frequency and damping ratio $f = 5$ Hz, $\xi = 5$, galvanometer's frequency and damping ratio $f = 10$ Hz, $\xi = 0.6$ and coupling coefficients $\sigma_1 = 0.01$, $\sigma_2 = 1$.

Fig. 14 presents $|\varepsilon(\omega)|$ in Eq. (41) for: sampling frequency 200 Hz; frequency range or the instrument correction requested: 0.05 Hz $\div$ 30 Hz; the transducer's frequency and damping ratio $f_{tr} = 5$ Hz, $\xi_{tr} = 5$ (velocity type); galvanometers frequency and damping ratio $f_{\text{galv}} = 10$Hz, $\xi_{\text{galv}} = 0.6$ (acceleration type); and coupling coefficients $\sigma_1 = 0.01$, $\sigma_2 = 1$. Fig. 15 shows the transfer function of the coupled transducer–galvanometer system with these parameters. As one can see the device is only a hypothetical one and has "poor" characteristics. It was chosen to make the effect of instrument correction more pronounced. Comparison of the last two figures shows that ICR2 performs well with accuracy of 3×10^{-3} in the range 0.09 Hz $< f <$ 27 Hz and with accuracy 10^{-1} in the ranges 0.065 Hz $< f <$ 0.09 Hz and 27 Hz $< f <$ 29 Hz. This means that the algorithm does reconstruct the amplitude characteristics of the motion far beyond the "flat" portion of the system response.

III.4 Case study

Another test performed is a case study. A typical strong motion accelerogram (Lee and Trifunac, 1987) was taken to represent the exact acceleration of the ground. This was the S50W component of the record obtained during the Imperial Valley earthquake in California, on October 15, 1979, at epicentral distance of 27 km (Fig. 16). The scheme of the testing procedure is presented by the flow chart in Fig. 17.

Eq. (2) was solved using the forth order Runge-Kutta method. This procedure simulates the work of the recording device. The parameters for the coupled system where the same as for the first test, discussed in Section III.3 and are summarized in Fig. 15. As one can see comparing Fig. 15 and Fig. 16b, the working range of the device adopted is narrower than the spectrum of the acceleration to be recorded. Prior to the integration of Eq. (2), the interpolation of the input record was performed. This was necessary because Runge- Kutta method becomes unstable if the process under consideration has the smallest period comparable with the time-step size used during the integration.

The record considered has 50 Hz sampling frequency and considerable Fourier amplitudes up to 15 Hz. The factor 50/15 = 3.3 appears not to be sufficient for the Runge-Kutta method to be stable. After interpolation with $k = 10$ (see section III.1.3, step #4), the safety factor becomes $(50/15) \cdot 10 = 33$, and the sampling frequency becomes $50 \cdot 10 = 500$Hz. The low-pass filter with cut off at 25 Hz (which is the original Nyquist frequency) should follow the interpolation to filter out all high frequencies that could be introduced during the interpolation. This step is necessary because the criterion $1/\rho_1 < 0.1$ from Fig. 10 was not satisfied. Here ρ_1 is the highest frequency (expressed in terms of the sampling frequency) that is present in the signal prior to interpolation: in our case it is $15/50 = 0.3$.

The interpolated and low-pass filtered ground acceleration was supplied as an input to Runge-Kutta integration. The resulting function φ_{500} is shown in Fig. 18 (bottom).

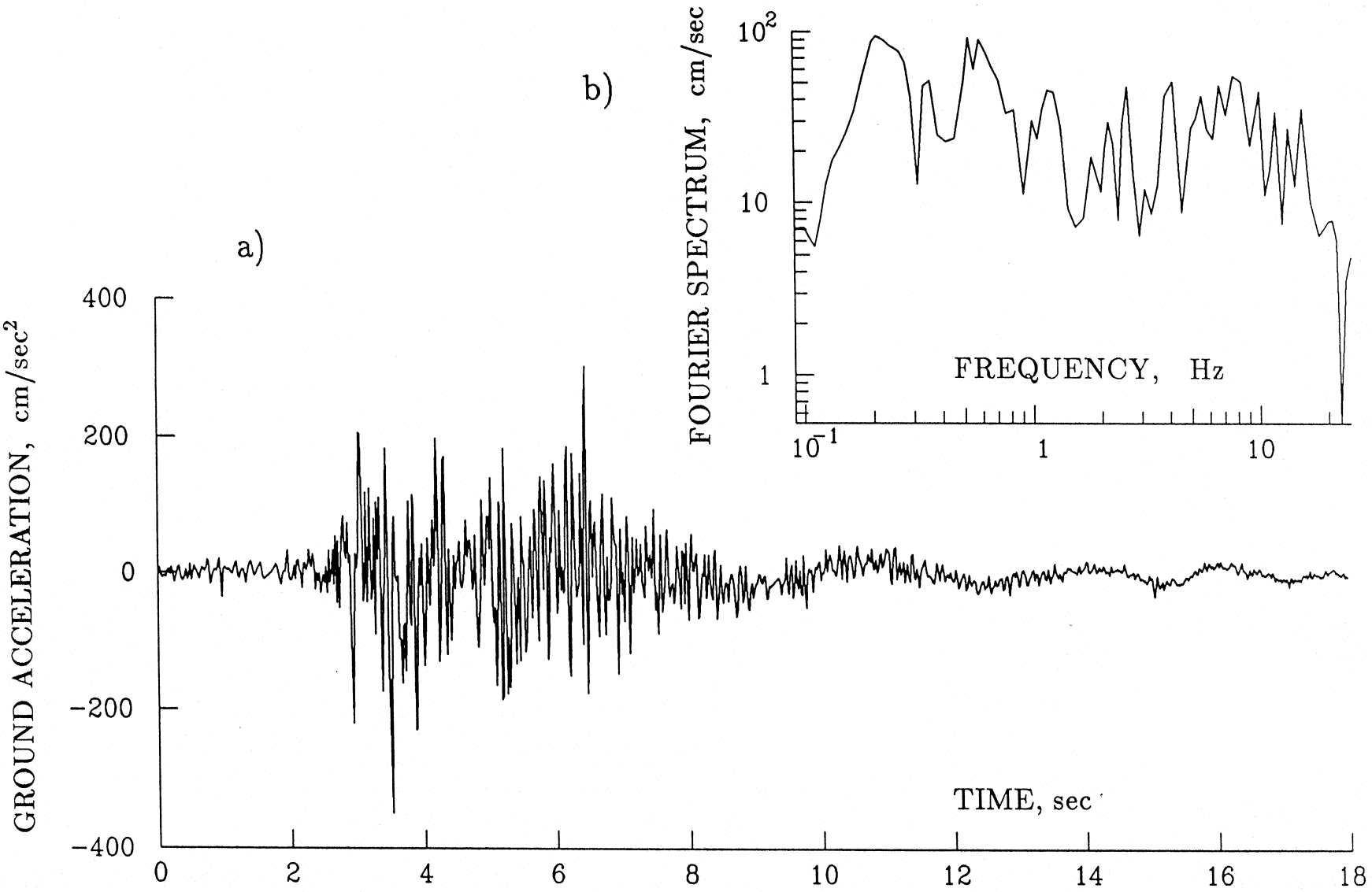

Fig. 16 S50W component (total length 37.9 sec) of the Imperial Valley earthquake in California (Oct. 15, 1979), recorded at epicentral distance 27 km; a) time history (first 18 sec), b) Fourier spectrum. This record was adopted as the exact absolute ground acceleration.

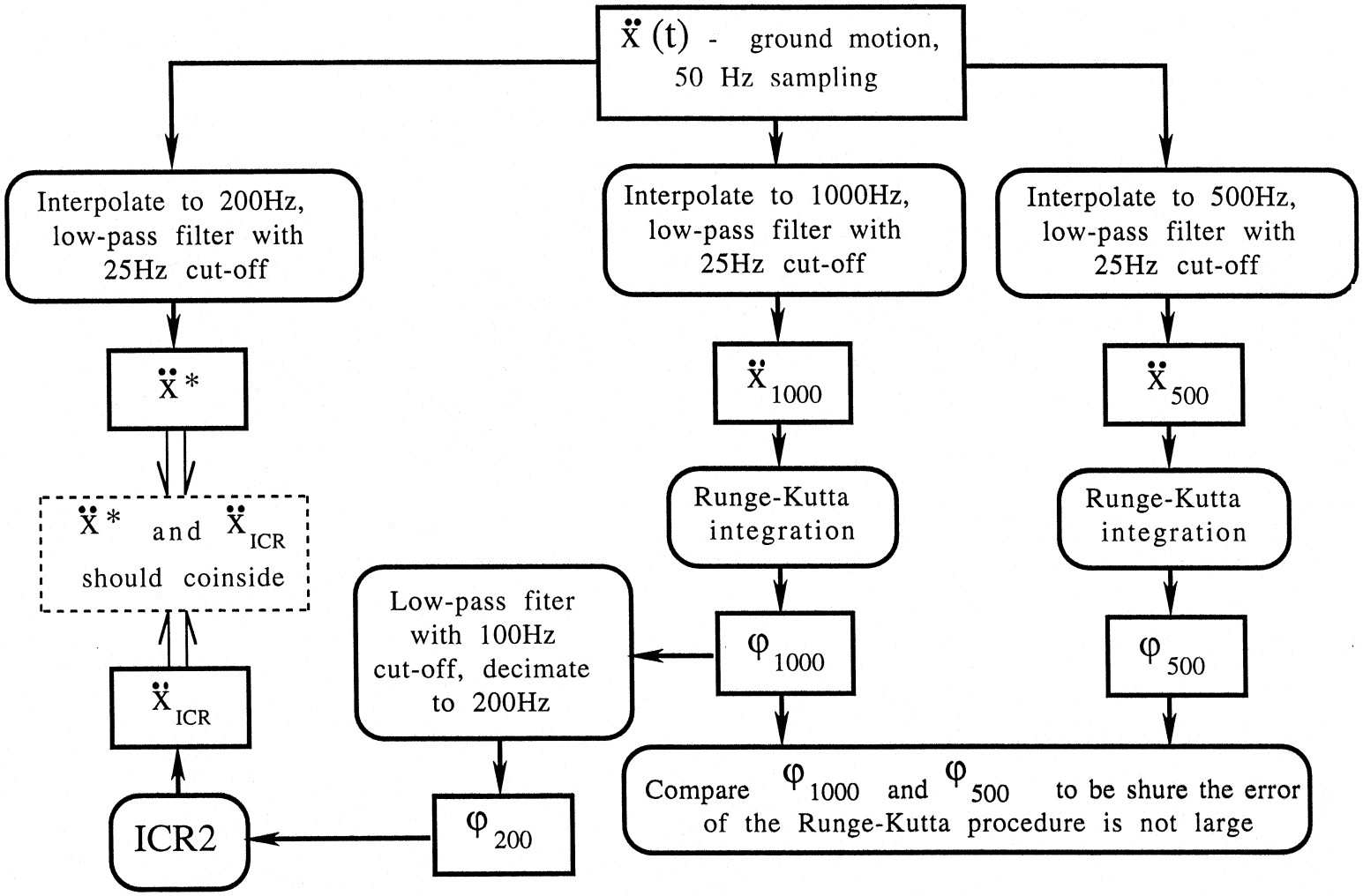

Fig. 17 Flow chart of the testing procedure for the case study.

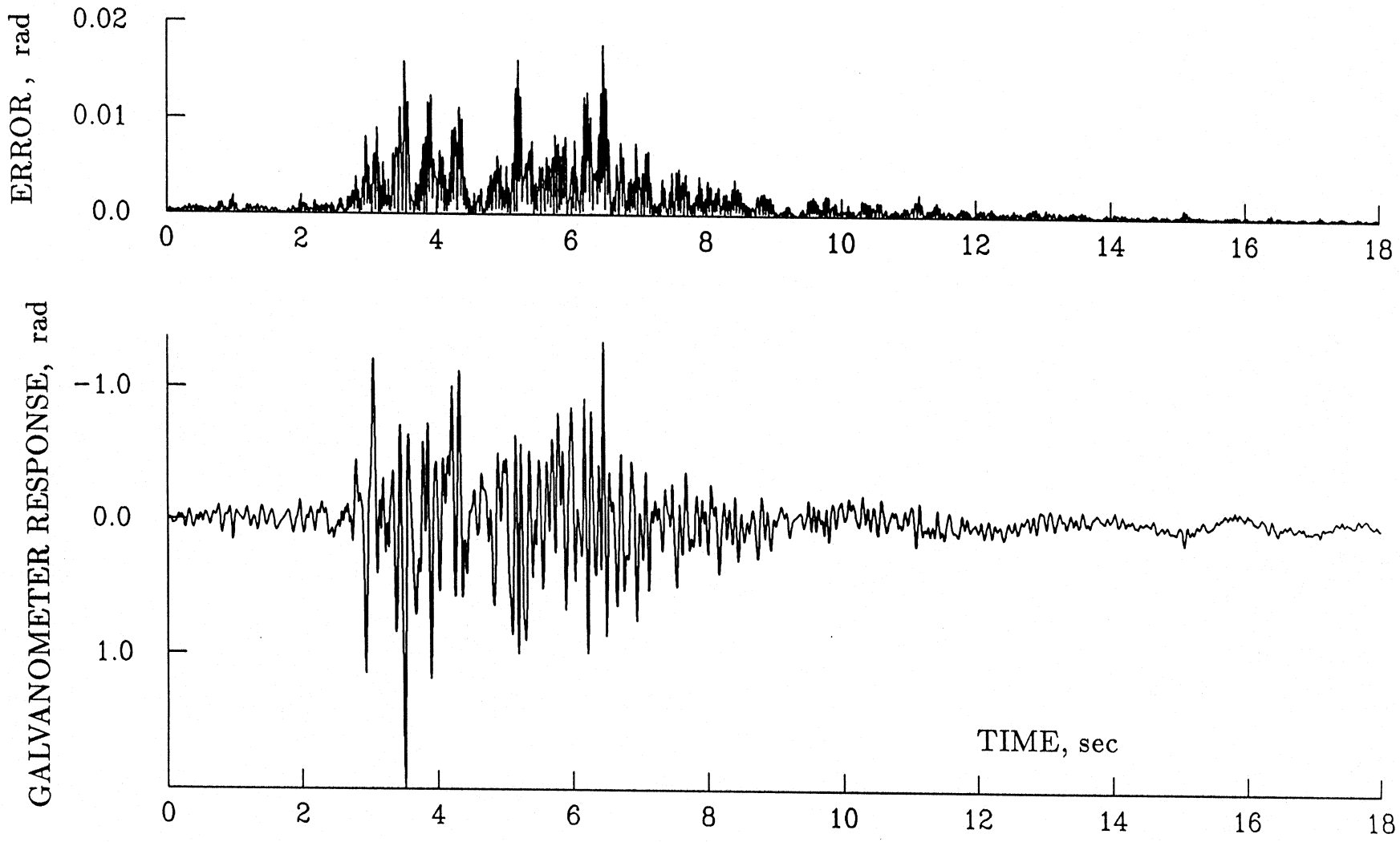

Fig. 18 Relative rotational response of the hypothetical device (with characteristics from Fig. 15) to the ground acceleration from Fig. 16, obtained by integration of Eq. (2) with sampling frequency 500 Hz (bottom), and the estimate of the absolute error (top).

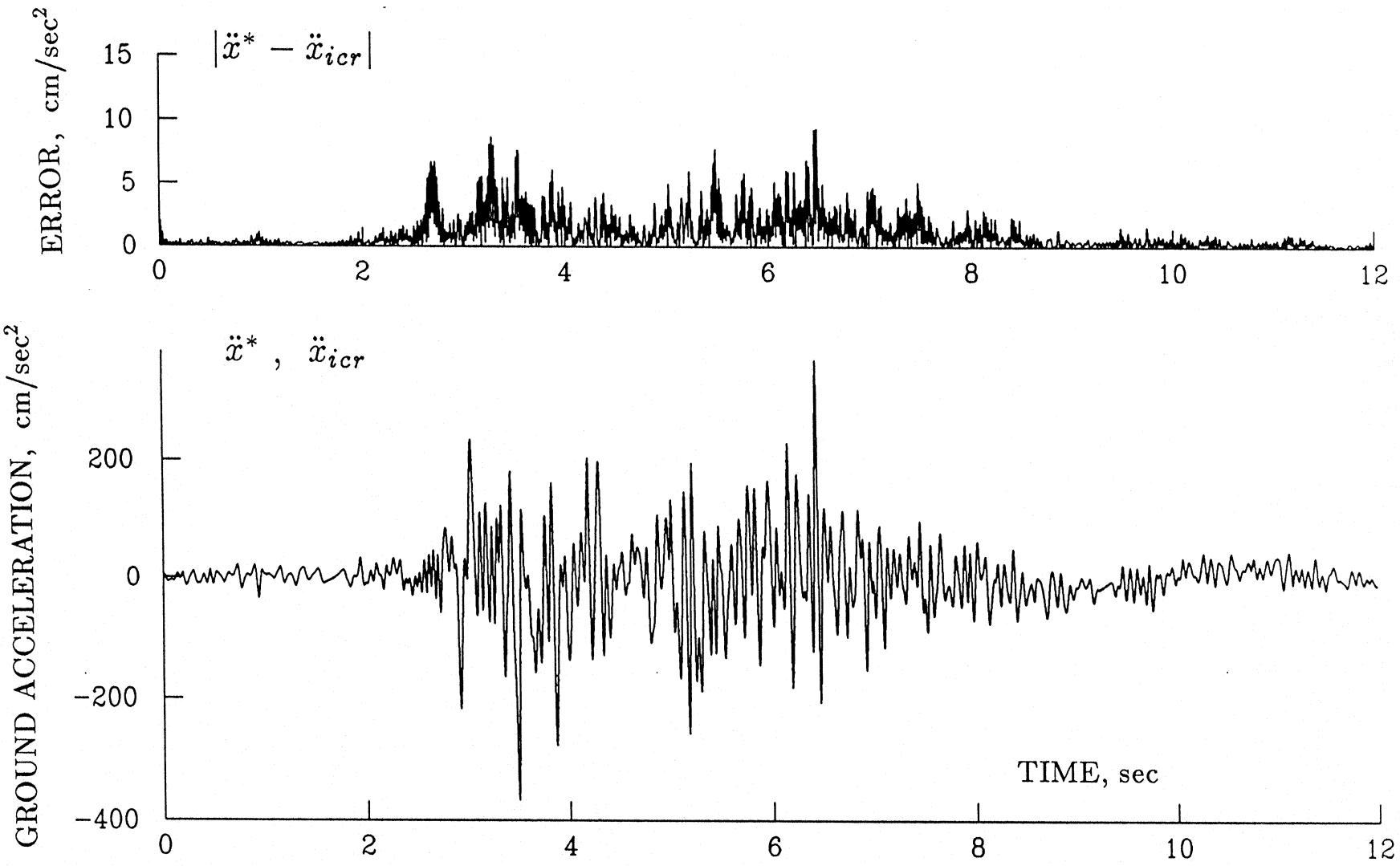

Fig. 19 Bottom: comparison of the exact ground acceleration $\ddot{x}^*$ (solid line) and the corrected acceleration after the ICR2 procedure $\ddot{x}_{\text{icr}}$ (dotted line). The two lines are practically indistinguishable. Top: the discrepancy $|\ddot{x} - \ddot{x}_{\text{icr}}|$ as a function of time.

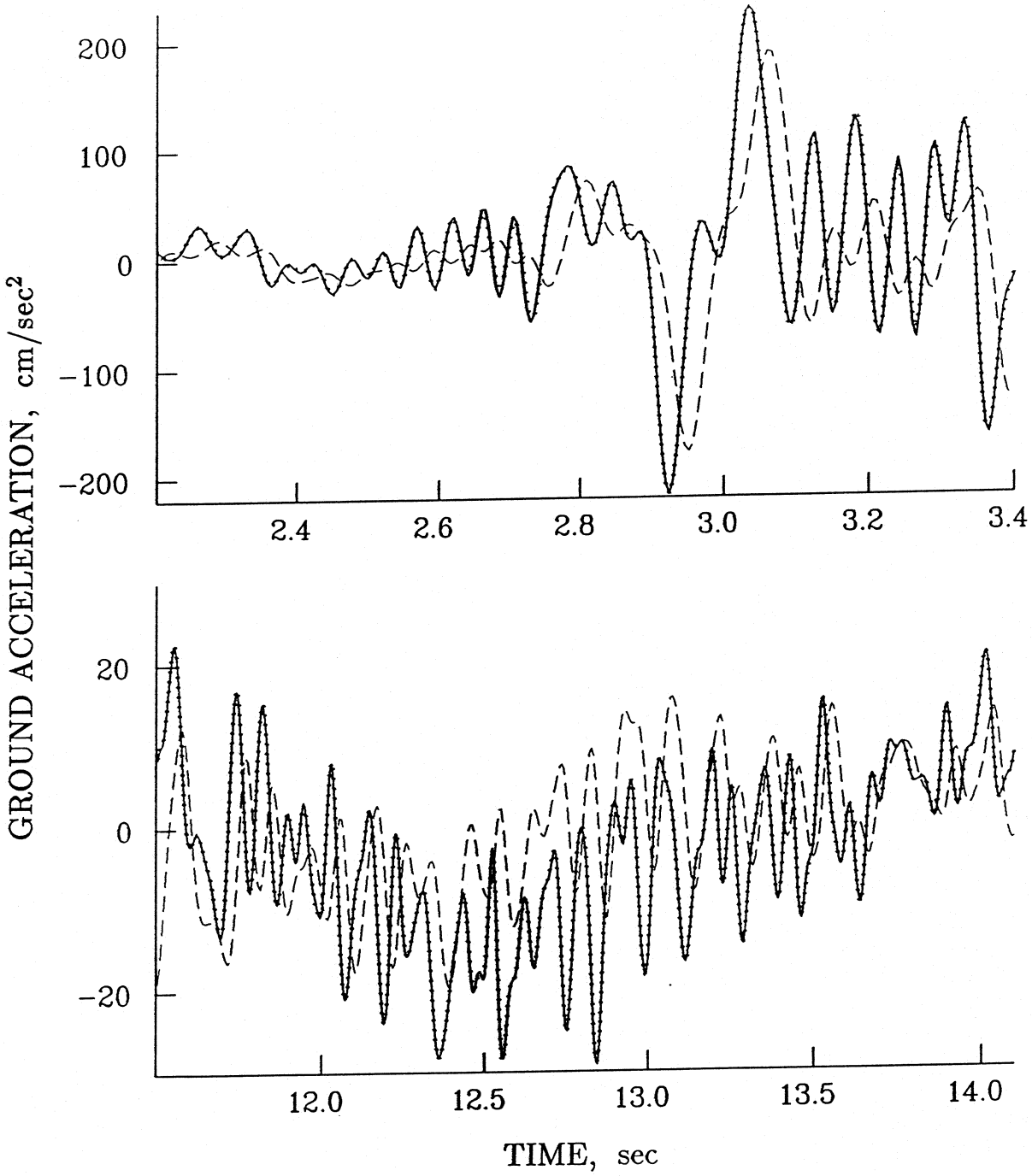

Fig. 20 The original (solid lines), properly scaled "recorded" (dashed lines) and reconstructed (dotted lines) acceleration. Two parts of the record are shown: with the intensive high frequency content (top) and with the substantial low frequency component (bottom).

The vertical axis in this figure is flipped to make the comparison with the exact input acceleration easier, (recall π shift in the phase for the "accelerometer" in Fig. 2b and 2c). The same procedure was repeated with the interpolation factor $k = 20$ and, therefore, sampling frequency 1000Hz, and φ_{1000} was obtained. The estimate of the error introduced by Runge-Kutta integration, can be obtained by comparison of φ_{500} and φ_{1000}. Relaying on the well-known estimation of the local error (Dahlquist and Björck, 1974), one can assume that the global error of φ_{500} should not exceed $|\varphi_{500} - \varphi_{1000}|$. (The latter is true if the function under consideration is smooth enough. In our case the record should have many points per period for the smallest period that is present in the record, which means that high sampling rate is required). Fig. 18 (top) shows $|\varphi_{500} - \varphi_{1000}|$ as a function of time and allows one to conclude that the accuracy of the integration of the Eq. (2) by the method chosen is approximately 10^{-2} for 500 Hz sampling frequency and not worse than that for 1000 Hz sampling frequency.

It is customary to perform the routine strong motion data digitization with sampling frequency 200 Hz (Lee and Trifunac, 1979a,b), so we reduced the sampling of φ_{1000} from 1000 Hz to 200 Hz by applying the decimation subroutine. Note, that prior to decimation, a low-pass filtering with cut-off at 100 Hz should be done. The output of these two procedures (function φ_{200}) was used as the representation of the response of the strong motion recording device that should be corrected by ICR2. Before continuing we compare Fig. 18 (bottom) and Fig. 16a and notice how the record is disturbed during the "recording process" in both high and low frequency parts of the spectrum. The working frequency range for the ICR2 was chosen to be $f_2 = 0.05$ Hz $< f < 25$ Hz $= f_1$. Then the corrected accelerogram, $\ddot{x}_{icr}$, should, ideally, coincide with the initial record $\ddot{x}$ (Fig. 16a). However, some additional steps should be done to make this comparison possible. These steps are: interpolation of $\ddot{x}$ to 200 Hz and low-pass filtering with 25 Hz cut off (we designate the result as $\ddot{x}^*$). Then the output of the instrument correction algorithm $\ddot{x}_{icr}$ and the "exact" interpolated accelerogram $\ddot{x}^*$ can be compared. These two functions are plotted on top of each other in Fig. 19 (bottom). As one can see, those appear the same to the naked eye, which means that the original ground acceleration was adequately reconstructed throughout the whole required frequency range. The difference between $\ddot{x}_{icr}$ and $\ddot{x}^*$ is shown in Fig. 19 (top). The accuracy of the result can be estimated as the ratio of the scales on Fig. 19 (top) and (bottom), which is $\approx 5 \times 10^{-2}$. Recalling the accuracy of the Runge-Kutta solution as 10^{-2}, we can assume that the difference $|\ddot{x}_{icr} - \ddot{x}^*|$ arises mostly from the instrument correction procedure. This allows us to conclude that in the case studied the relative error of the ICR2 is approximately 5×10^{-2}, which is reasonable. The largest error appears at the time intervals with highest frequency content. The most rich in high frequencies part of the record is shown in Fig. 20 (top), and the low frequency interval is presented in the bottom of this figure. All three curves: original acceleration $\ddot{x}^*$ (solid line), the properly scaled "recorded" acceleration φ_{200} (dashed lines) and the corrected signal $\ddot{x}_{icr}$ (dotted lines) are shown together for comparison.

IV. CONCLUSIONS

The main results of the work presented can be summarized as follows:

1. The need for accurate representation of both phase and amplitude of the original motion being measured requires correction of the direct output from coupled transducer–galvanometer systems for the instrument response. This procedure not only significantly increases the frequency band beyond "flat" portion of the amplitude response, but it also corrects the phase, which always depends on frequency for the system considered.

2. The proposed instrument correction algorithm involves numerical differentiations and integrations in time domain and can be applied to the output from any coupled system which can be described by Eq. (2). It is not necessary to design instruments so that their output is proportional to displacement, velocity or acceleration of the moving point, if the direct output from the system is corrected by the proposed procedure. It is also not necessary to worry about small coupling between devices if it is more convenient to design an instrument with big coupling coefficient.

3. The tests we presented show that the relative error of the procedure is about 5% inside the frequency band which was chosen to be corrected for instrument response. In the case study considered, this frequency band was much broader than the "flat" portion of the "device", "recording" the motion (the "recording" was modeled by Runge-Kutta integration of the governing Eq. (2)).

4. The program written on the basis of the proposed algorithm can be integrated into standard packages of strong motion and seismological data processing programs, and a great number of records obtained by coupled transducer–galvanometer systems can be corrected for the instrument response.

V. REFERENCES

Amini, A., M.D. Trifunac and R.L. Nigbor (1987). A Note on the Noise Amplitudes in Some Strong Motion Accelerographs, Soil Dynamic and Earthquake Eng. Vol. 6, No. 3, 180–185.

Borisevich, E.S.; (Editor) (1981). Katalog Geofizicheskoi Apparaturi, "Nauka", Moscow, (in Russian).

Cappellini, V., Constantinides, A.G. and Emiliani, P. (1978). Digital Filters and Their Applications, Academic Press Inc., London.

Crochiere, R.E. and Lawrence, R.R. (1975). Optimum FIR Digital Filter Implementations for Decimation, Interpolation, and Narrow-band Filtering, IEEE Transactions on Acoustics, Speech, and Signal Processing, Vol. ASSP-23, No. 5., 444–456.

Dahlquist, G. and Björck, A. (1974). Numerical Methods, N.J.: Prentice-Hall.

Galitzin, B. (1912). Lektzii po Seismometrii, St. Peterburg, (in Russian).

Hamming, R.W. (1983). Digital Filters, N.J.: Prentice-Hall.

Khalturin, V.I. (1991). Personal Communications.

Lee, V.W. and Trifunac, M.D. (1979a). Automatic Digitization and Processing of Strong Motion Accelerograms, Part I – Automatic Digitization, Department of Civil Engineering, Report No. 79-15 I, University of Southern California, Los Angeles, California.

Lee, V.W. and Trifunac, M.D. (1979b). Automatic Digitization and Processing of Strong Motion Accelerograms, Part II – Computer Processing of Accelerograms, Department of Civil Engineering, Report No. 79-15II, University of Southern California, Los Angeles, California.

Lee, V.W. and Trifunac, M.D. (1984). Current Developments in Data Processing of Strong Motion Accelerograms, Department of Civil Engineering, Report No. 84-01, University of Southern California, Los Angeles, California.

Lee, V.W. and Trifunac, M.D. (1987). Strong Earthquake Ground Motion Data In EQINFOS: Part I, Department of Civil Engineering, Report No. 87-01, University of Southern California, Los Angeles, California.

Lee, V.W. and Trifunac, M.D. (1990). Automatic Digitization and Processing of Accelerograms Using Personal Computers, Department of Civil Engineering Report No. 90-03, Univ. of Southern California, Los Angeles, California.

Lee, V.W. and Trifunac, M.D. and A. Amini (1982). Noise in Earthquake Accelerograms, ASCE, EM6, Vol. 108, 1121–1129.

Lee, V.W., Wang, Y.Y. (1983). On the Instrument correction of the RDZ-1 Strong-Motion Pendulum Galvanometer in China, Earthquake Engineering and Engineering Vibration, Vol. 3, Part 4, Dec. 25–35, (in Chinese).

Medvedev, S.V. (1962). Inženernaya Sejsmologia, State Publishing of the Civil Engineering, Architectural and Building Materials Literature, Moscow, (in Russian).

Mintzer, F. and Liu, B. (1978). The Design of Optimal Multirate Band-Pass and Band-Stop Filters, IEEE Transactions on Acoustics, Speech and Signal Processing Vol. ASSP-26, No. 6., 534–543.

Oetken, G., Parks, T.W. and Schüssler, H.W. (1975). New Results in the Design of Digital Interpolators, IEEE Transactions on Acoustics, Speech and Signal Processing, Vol. ASSP-23, No. 3., 301–309.

Press, W.H., Flannery, B.P., Teukolsky, S.A. and Vetterling W.T. (1986). Numerical Recipes: The Art of Scientific Computing, Cambridge University Press.

Savarensky, E.F. and Kirnos, D.P. (1955). Elements of Seismology and Seismometry, Part II – Elements of Seismometry (by Kirnos, D.P.), Moscow.

Shively, R.R. (1975). On Multistage Finite Impulse Response (FIR) Filters with Decimation, IEEE Transactions on Acoustics, Speech and Signal Processing, Vol. ASSP-23, No. 4., 353–357.

Trifunac, M.D. (1971). Zero Baseline Correction of Strong-Motion Accelerograms, Bulletin of the Seismological Society of America, Vol. 61, No. 5, 1201–1211.

Trifunac, M.D. (1972). A Note on Correction of Strong-Motion Accelerograms for Instrument Response, Bulletin of the Seismological Society of America, Vol. 62, No. 1, 401–409.

Trifunac, M.D., F.E. Udwadia and A.G. Brady (1973). Analysis of Errors in Digitized Strong-Motion Accelerograms, Bulletin of the Seismological Society of America, Vol. 63, 157–187.